Article

Cell Reports

Disease-Linked Glutarylation Impairs Function and Interactions of Mitochondrial Proteins and Contributes to Mitochondrial Heterogeneity

Graphical Abstract

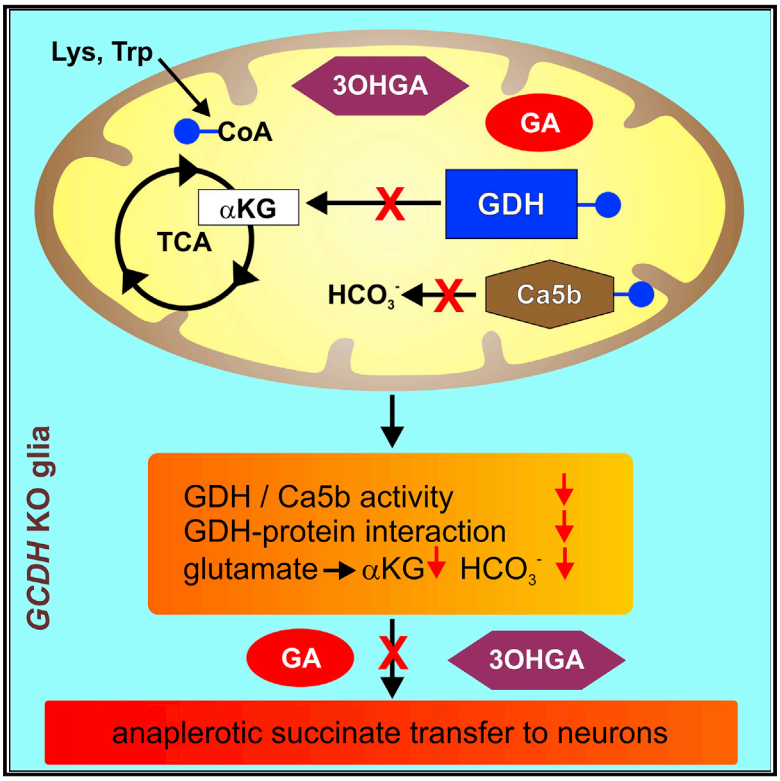

Authors

Jessica Schmiesing, Stephan Storch, Ann-Cathrin Dörfler, ..., Abdul Waheed, William S. Sly, Thomas Braulke

Correspondence

braulke@uke.de

In Brief

Schmiesing et al. show that the lack of GCDH results in glutarylation of mitochondrial proteins in glial cells affecting amino acid metabolism and the tricarboxylic acid cycle. They identify glutamate dehydrogenase as a target suppressed by glutarylation that is linked to glial glutamate metabolism and anaplerosis in GCDH-deficient neuronal cells.

Highlights

- Glutaryl-CoA dehydrogenase (GCDH) defects increase mitochondrial glutaryl-CoA level
- Glutarylated mitochondrial proteins accumulate in glial cells of GCDH KO mice
- Glutarylation suppresses GDH activity and protein interactions
- Affected glutamate metabolism links lysine glutarylation with neuronal anaplerosis

Data and Software Availability

PXD007881

Schmiesing et al., 2018, Cell Reports *24*, 2946–2956
September 11, 2018 © 2018 The Author(s).
https://doi.org/10.1016/j.celrep.2018.08.014

CellPress

OPEN ACCESS
CellPress

Cell Reports
Article

Disease-Linked Glutarylation Impairs Function and Interactions of Mitochondrial Proteins and Contributes to Mitochondrial Heterogeneity

Jessica Schmiesing,[1] Stephan Storch,[1] Ann-Cathrin Dörfler,[1] Michaela Schweizer,[2] Georgia Makrypidi-Fraune,[1] Melanie Thelen,[3] Marc Sylvester,[3] Volkmar Gieselmann,[3] Catherine Meyer-Schwesinger,[4] Friedrich Koch-Nolte,[5] Henning Tidow,[6] Chris Mühlhausen,[1] Abdul Waheed,[7] William S. Sly,[7] and Thomas Braulke[1,8,*]

[1]Department of Biochemistry, Children's Hospital, University Medical Center Hamburg-Eppendorf, 20246 Hamburg, Germany
[2]Center of Molecular Neurobiology, University Medical Center Hamburg-Eppendorf, 20246 Hamburg, Germany
[3]Institute of Biochemistry and Molecular Biology, University of Bonn, 53115 Bonn, Germany
[4]Department of Internal Medicine III, Nephrology and Rheumatology, University Medical Center Hamburg-Eppendorf, 20246 Hamburg, Germany
[5]Institute of Immunology, University Medical Center Hamburg-Eppendorf, 20246 Hamburg, Germany
[6]The Hamburg Center for Ultrafast Imaging & Department Chemistry, University Hamburg, 20146 Hamburg, Germany
[7]Department of Biochemistry and Molecular Biology, Edward A. Doisy Research Center, Saint Louis University School of Medicine, St. Louis, MO 63104, USA
[8]Lead Contact
*Correspondence: braulke@uke.de
https://doi.org/10.1016/j.celrep.2018.08.014

SUMMARY

Lysine glutarylation (Kglu) of mitochondrial proteins is associated with glutaryl-CoA dehydrogenase (GCDH) deficiency, which impairs lysine/tryptophan degradation and causes destruction of striatal neurons during catabolic crisis with subsequent movement disability. By investigating the role of Kglu modifications in this disease, we compared the brain and liver glutarylomes of Gcdh-deficient mice. In the brain, we identified 73 Kglu sites on 37 mitochondrial proteins involved in various metabolic degradation pathways. Ultrastructural immunogold studies indicated that glutarylated proteins are heterogeneously distributed in mitochondria, which are exclusively localized in glial cells. In liver cells, all mitochondria contain Kglu-modified proteins. Glutarylation reduces the catalytic activities of the most abundant glutamate dehydrogenase (GDH) and the brain-specific carbonic anhydrase 5b and interferes with GDH-protein interactions. We propose that Kglu contributes to the functional heterogeneity of mitochondria and may metabolically adapt glial cells to the activity and metabolic demands of neighboring GCDH-deficient neurons.

INTRODUCTION

The degradation of lysine, hydroxylysine, and tryptophan proceeds initially via separate pathways and converges into a common pathway at the point of 2-oxoadipic acid in mitochondria. This intermediate is converted to glutaryl-coenzyme A (glu-CoA) by the 2-oxoglutarate (α-ketoglutarate) dehydrogenase complex and then oxidatively decarboxylated to crotonyl-coenzyme A catalyzed by the mitochondrial matrix protein glutaryl-CoA-dehydrogenase (GCDH). The enzymatically active GCDH exists as homotetramer containing four flavin adenine dinucleotide (FAD) groups (Goodman et al., 1995). In addition to homotetramerization, GCDH can interact with various other mitochondrial proteins that seem to constitute multimeric dehydrogenase complexes required for efficient metabolism of glutaryl-CoA (Schmiesing et al., 2014).

Mutations in the *GCDH* gene cause the neurometabolic disorder glutaric aciduria type 1 (GA1), typically associated with the accumulation of glutaric acid (GA) and 3-hydroxyglutaric acid (3OHGA) in body fluids and tissues. GA1 patients are prone to the development of encephalopathic crises triggered by catabolic stress induced by fever, infections, vomiting, and/or diarrhea. During catabolic crises, concentrations of the metabolites GA and 3OHGA show a further increase. The development of an encephalopathic crisis is accompanied by destruction of striatal neurons with a subsequent irreversible disabling movement disorder. Children affected by GA1 are at risk for such a crisis during a time window from 3 to 36 months of age (Goodman and Frerman, 2001). A *Gcdh*-deficient mouse model displays biochemical and histopathological symptoms resembling observations in GA1 patients (Koeller et al., 2002), and the administration of a high-protein diet (HPD) to 4- to 6-week-old *Gcdh* knockout (KO) mice leads to the development of metabolic crises, with further increase in GA and 3OHGA concentrations, vacuolization in the brain, paralysis, seizures, and renal proximal tubule alterations (Keyser et al., 2008; Thies et al., 2013; Zinnanti et al., 2006).

The molecular and physiological mechanisms underlying the pathogenesis of GA1 are poorly understood. We reported that glutaryl-CoA serves as a substrate for lysine glutarylation (Kglu) reactions and that *Gcdh* KO mice show increased amounts of glutarylated proteins in liver tissue (Tan et al., 2014). Protein

This is an open access article under the CC BY-NC-ND license (http://creativecommons.org/licenses/by-nc-nd/4.0/).

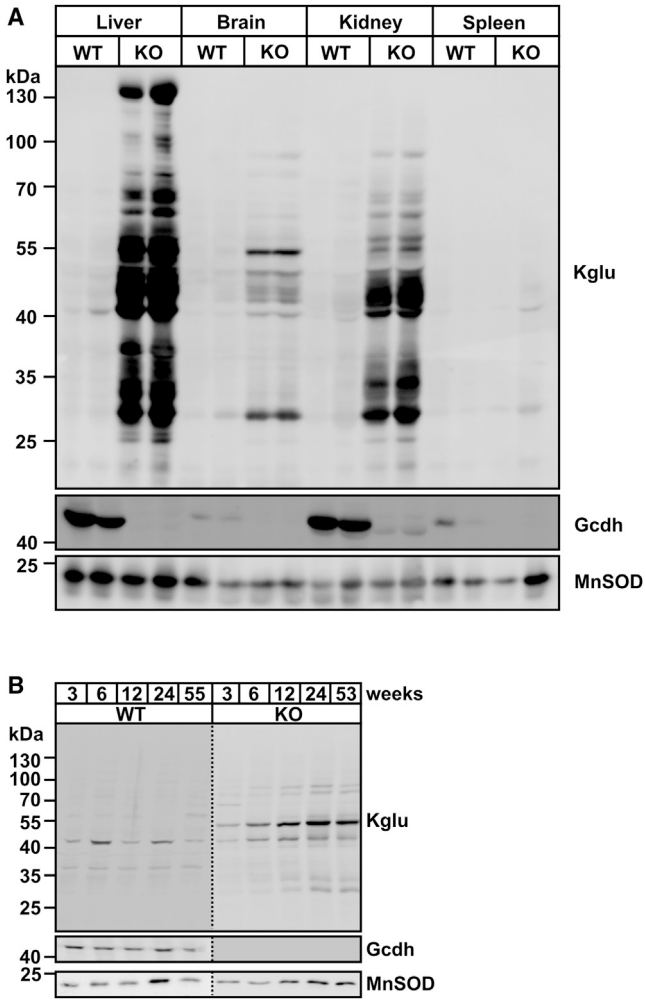

Figure 1. Lysine Glutarylation in WT and *Gcdh* KO Mouse Tissues

(A) Kglu western blot analysis of liver, brain, kidney, and spleen mitochondrial extracts from WT and *Gcdh* KO mice. Gcdh and MnSOD expression were used as controls.

(B) Age dependency of protein glutarylation in extracts of brain mitochondria from WT and *Gcdh* KO mice.

See also Figure S1.

glutarylation is a non-enzymatic process that is reversible by the NAD^+-dependent sirtuin 5 deacylase (SIRT5) (Tan et al., 2014). Proteomic analysis of livers from *Sirt5* KO mice revealed 191 glutarylated proteins, of which the most highly modified carbamoylphosphate synthase 1 (CPS1, 33 sites) exhibits reduced activity in both *Sirt5* KO and *Gcdh* KO livers (Tan et al., 2014).

Here, we analyzed glutarylation of proteins in various tissues and cultured cells of *Gcdh* KO mice and identified 37 glutarylated mitochondrial proteins in the brain, the most affected organ in GA1 patients during catabolic crisis; in contrast, 154 mitochondrial proteins were found to be modified in the liver. We showed that the catalytic activity of two enzymes, glutamate dehydrogenase (GDH) and carbonic anhydrase 5B (Ca5b), and protein-protein interactions were significantly reduced by glutarylation.

RESULTS

Tissue- and Protein-Dependent Glutarylation in *Gcdh* KO Mice

We observed a dramatic increase in global protein glutarylation in mitochondrial fractions of *Gcdh* (KO) mouse liver (Tan et al., 2014). Because catabolic crises both in GA1 patients and in *Gcdh* KO mice lead to severe striatal neurodegeneration and pathological changes in the kidney (Keyser et al., 2008; Kölker et al., 2015; Thies et al., 2013; Zinnanti et al., 2006), we investigated the protein glutarylation pattern in mitochondrial extracts from wild-type (WT) and *Gcdh* KO brains in comparison with liver, kidney, and spleen. Figure 1A demonstrates the specific and general elevation of protein glutarylation in *Gcdh* KO liver and kidney, with few tissue-dependent differences in distinct proteins. The extent of protein glutarylation was generally lower in brain tissue, where we detected 55 and 27 kDa polypeptides as the most prominent modified proteins. In spleen mitochondrial extracts of *Gcdh* KO mice, no protein glutarylation was observed (Figure 1A). The first glutarylated proteins were detected in 3-week-old *Gcdh* KO mouse brains (Figure 1B) and livers (Figure S1A), with a similar pattern but higher intensity at an age of 6 weeks up to 1 year.

Induced Metabolic Crisis Does Not Affect Protein Glutarylation in *Gcdh* KO Mice

Metabolic crisis induced by HPD in *Gcdh* KO mice leads to various alterations of biochemical, metabolic, and morphological parameters (Keyser et al., 2008; Thies et al., 2013; Zinnanti et al., 2006). To examine the effect of induced metabolic crisis, the protein glutarylation pattern was measured in mitochondrial extracts from brain and liver after a 4-day administration of normal diet (ND) and HPD in 6-week-old WT and *Gcdh* KO mice. As expected, we observed no effect of HPD on protein glutarylation in WT brain (Figure 2A) and liver (Figure S1B), and the pattern and intensity of glutarylated proteins after ND or HPD in *Gcdh* KO mice was unchanged. Consequently, western blot analysis revealed no effects of HPD administration on Sirt5 expression (Figure 2B; Figure S1C), excluding crisis-dependent differences in deglutarylation activity between WT and *Gcdh* KO mice.

Glutarylated Proteins Are Enriched in *Gcdh* KO Mitochondria

We applied post-embedding immunogold transmission electron microscopy to visualize the subcellular localization of glutarylated proteins in sections of *Gcdh* KO mouse brain (Figure 3A; Figure S2A) and liver (Figures S2B and S3A). Immunogold staining confirmed the accumulation of glutarylated proteins in mitochondria of *Gcdh* KO brain cells, but not in WT controls. Higher magnifications (Figure 3A, right panel) showed a distribution of gold particles along the cristal membrane. Surprisingly, mitochondria in neurons (red and green underlined; indicated by the synaptic contact zones) lack immunogold staining, whereas the mitochondrial Kglu-labeled proteins in *Gcdh* KO brains appear to be restricted to the surrounding glial cells (Figure 3A). The distribution of anti-Kglu-protein A immunogold particles (10 nm) was determined on images randomly taken from ultrathin cerebellar sections at 20,000× magnification. From

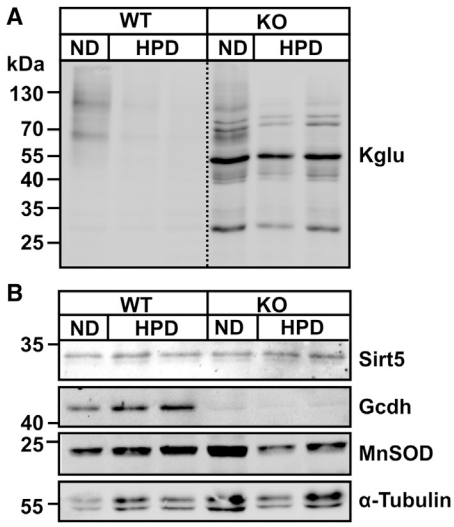

Figure 2. No Effect of Induced Metabolic Crisis on Protein Glutarylation in Brain Tissue of *Gcdh* KO Mice

(A) Protein glutarylation was visualized in extracts of brain mitochondrial fractions of 6-week-old WT and *Gcdh* KO mice by Kglu immunoblotting. The mice were fed with normal (ND) or high protein diet (HPD) for four days.

(B) Sirt5 western blot analysis of brain mitochondrial extracts prepared from WT and *Gcdh* KO mice under normal (ND) or high protein diet (HPD). Gcdh, MnSOD, and α-tubulin expression were used as controls.

See also Figure S1.

217 mitochondria, 24 were found to be positive (>2 gold particles) in cellular compartments lacking clear synaptic contacts (Figure S2A). This finding is corroborated by immunofluorescence double labeling for glutarylated proteins and ATP synthase subunit beta (Atp5b), a mitochondrial marker protein, being co-localized in some mitochondria from cells surrounding Kglu-negative Purkinje cells in the *Gcdh* KO cerebellum (Figure 3B). Moreover, double immunofluorescence labeling for glutarylated proteins and glial fibrillary acidic protein (GFAP), a marker protein for astrocytes, revealed strict localization of Kglu-positive proteins in Bergmann glial processes (Figure 3C), whereas neuron-specific nuclear protein (NeuN)-positive Purkinje cells lack Kglu staining (Figure 3D).

Immunogold labeling of glutarylated proteins was even stronger in ultrathin sections of *Gcdh* KO liver sections and distributed highly along the cristal membrane of all hepatic mitochondria (Figures S2B and S3A). Few immunogold particles were found within small empty vacuolar structures in both WT and *Gcdh* KO sections, which are most likely due to unspecific binding of the antibody.

In vitro glutarylation by incubation of subcellular liver extracts with an excess of glutaryl-CoA failed to modify significantly cytosolic proteins, whereas almost identical patterns and intensities of *in vitro* glutarylated proteins were detected in mitochondrial lysates of WT and *Gcdh* KO mice, indicating that protein glutarylation is limited by the glutaryl-CoA concentration (Figure S3B). The few proteins found to be glutarylated to a low extent in the cytosolic fraction of *Gcdh* KO mice originate most likely by mitochondrial disruption, shown by the presence of traces of the mitochondrial marker protein manganese-dependent superoxide dismutase (MnSOD) in the cytosolic fraction (Figure S3B). It is not known whether structural requirements in cytosolic and mitochondrial proteins are responsible for suitability to serve as targets for glutarylation.

Western blotting analysis of cultured hepatocytes also demonstrated high amounts of glutarylated proteins in *Gcdh* KO cells, but not in WT cells (Figure S3C). Double immunofluorescence microscopy showed the complete co-localization of Kglu-positive proteins with Atp5b in *Gcdh* KO hepatocytes (Figure S3D).

Proteome-wide Screening of Kglu Substrates in *Gcdh* KO Mouse Brain and Liver

To identify targets of protein glutarylation, we performed proteomic profiling using brain and liver of 6-week-old *Gcdh* KO mice, which show low- and high-protein glutarylation patterns, respectively (Figure 1A). Using the anti-glutaryl-peptide antibody enrichment and mass spectrometry (MS) strategy depicted in Figure 4A, we identified 73 Kglu sites on 37 mitochondrial proteins of the brain and 425 Kglu sites on 154 mitochondrial proteins of the liver (Figure 4B; Table S1), with a less than 1% false discovery rate (FDR) on peptide level using Proteome Discoverer software. The MS dataset has been deposited to the Proteome Xchange Consortium (Vizcaíno et al., 2014) via PRIDE: PXD007881. Thirty-two proteins were glutarylated in both brain and liver mitochondria of *Gcdh* KO mice (Figure 4B; Table 1). Approximately 80% of the Kglu proteins in the brain contained only one or two Kglu sites, whereas five (14%) were glutarylated at more than three sites, such as glutamate dehydrogenase 1 (Gdh, 11 sites), aconitate hydratase (Aco2, 6 sites), and citrate synthase (Cs, 4 sites) (Figure 4C; Table 1). We found five proteins, succinyl CoA:3-ketoacid CoA transferase 1 (Scot-s), carbonic anhydrase 5B (Ca5b), isocitrate dehydrogenase gamma 1 (Icdh subunit alpha), NAD kinase 2 (Nadk2), and presequence protease (Pitrm1), glutarylated only in the brain, but not in the liver, of *Gcdh* KO mice (Table S1). Most mitochondrial matrix proteins in the brain of *Gcdh* KO mice are not Kglu modified.

About two-thirds of glutarylated liver proteins contained one or two Kglu sites, whereas four (3%) were heavily glutarylated, such as carbamoyl-phosphate synthase 1 (Cps1, 36 sites), 3-ketoacyl-CoA thiolase (Acaa2, 14 sites), glutamate dehydrogenase (Gdh, 14 sites), and aspartate aminotransferase (Got2, 12 sites) (Figure S4A; Table S1). With the exception of Gdh, Acaa2 and Got2 were found to be glutarylated in brain at one site, whereas Cps1 was not detected (Table S1). In total, for 122 proteins that we found to be glutarylated in liver, no Kglu-modified peptides could be detected in the brain of *Gcdh* KO mice. It is likely that differences in the steady-state concentrations of glutaryl-CoA and the abundance of mitochondrial matrix proteins are responsible for the different number of targets and extent of modified lysine residues in brain and liver.

To assess whether any pathways might be coordinately regulated by Kglu-modified mitochondrial proteins in brain cells, we conducted a Kyoto Encyclopedia of Genes and Genomes (KEGG) enrichment analysis. This revealed that annotations of various mitochondrial metabolic pathways were enriched, including valine, leucine, and isoleucine and fatty acid

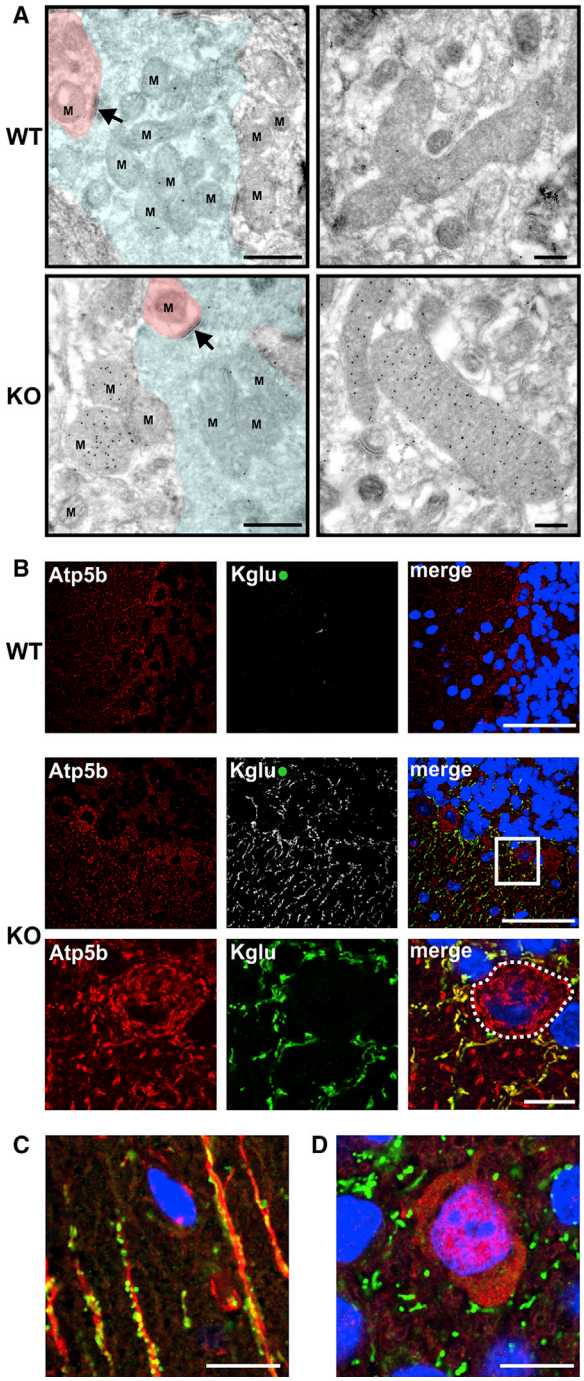

Figure 3. Localization of Glutarylated Proteins in Brain Tissue of WT and *Gcdh* KO Mice

(A) Representative ultrathin sections prepared by cryosectioning of cerebellar tissue from WT and *Gcdh* KO mice and anti-Kglu immunogold labeling. Arrows indicate the synaptic contact between presynaptic bouton (light green) and dendrite (light red). M, mitochondria. Scale bars: 500 nm comprehensive view, 250 nm magnified view.

(B) Immunofluorescence staining of glutarylated proteins (Kglu, green) on cerebellar sections derived from WT and *Gcdh* KO mice. Co-immunofluorescence staining shows co-localization with mitochondrial marker protein Atp5b (red). Nuclei were stained with Draq5 (blue). The Purkinje cell body is highlighted by a dashed circle. Scale bars: 50 μm comprehensive view, 10 μm magnified view.

(C) Co-immunofluorescence staining of glutarylated proteins (Kglu, green) and GFAP-positive Bergmann glia processes (red) on *Gcdh* KO cerebellar sections. Scale bar: 10 μm.

(D) Lack of co-immunofluorescence staining of glutarylated proteins (Kglu, green) in NeuN-positive Purkinje cells (red) on *Gcdh* KO cerebellar sections. Scale bar: 10 μm.

See also Figures S2 and S3.

degradation, as well as carbon metabolism and the tricarboxylic acid (TCA) cycle (Figure 4D; Table S2A). Similarly, in liver of *Gcdh* KO mice, the Kglu-modified proteins were involved in pathways of amino acid degradation and metabolism, butanoate, propanoate, and fatty acid metabolism, as well as the TCA cycle (Figure S4B; Table S2B).

Glutarylation Impairs GDH Activity and Protein Interactions

To determine whether protein glutarylation has a functional consequence, we analyzed two proteins, the most highly glutarylated glutamate dehydrogenase (Gdh) in the brain and the carbonic anhydrase 5B (Ca5b) that is glutarylated only in the brain (Table S1).

To analyze glutarylation under more standardized conditions, we chemically glutarylated bovine GDH with increasing concentrations of glutaryl-CoA (glu-CoA) for 4 hr (Figure S5). Under these conditions, half-maximum Kglu modifications of 55 kDa GDH was reached at a concentration of approximately 0.25 mM glu-CoA, showing the same electrophoretic mobility as the major Kglu-modified protein in mitochondrial fractions of *Gcdh* KO brain (Figure S5A, lanes 5 and 6). An almost identical Kglu pattern of mitochondrial proteins modified in *Gcdh* KO brain *in vivo* (lane 6) was detectable when we incubated the same fraction with 0.5 mM glutaryl-CoA (lane 10). With a few exceptions, the Kglu protein pattern of *Gcdh* KO brain mitochondria is similar to that of WT mitochondria modified *in vitro* in the presence of 0.5 mM glutaryl-CoA (lane 10 versus lane 9). Glutarylation of GDH *in vitro* resulted in the appearance of a single Kglu/GDH-positive band with a isoelectric point (pI) of 5.3 after isoelectric focusing (Figure 5A). These data suggest a uniform glutarylation extent at multiple sites under *in vitro* conditions. Time- and glu-CoA-dependent *in vitro* assays of GDH followed by MS confirmed these data. Incubation of GDH for 1 to 4 hr at 5 mM glu-CoA (Figures S5B and S5C) or for 4 hr in the presence of 0.5, 1.0, or 5.0 mM glu-CoA (Figures S5B and S5D) resulted in an increase in Kglu immunoreactivity. In total, we found 17 lysine residues glutarylated in GDH *in vitro*, of which seven were also modified *in vivo* (Table S3). However, 10 and 7 sites glutarylated *in vitro* were not detected in mitochondria of brain and liver tissue of *Gcdh* KO mice, respectively. Almost all sites were found to be glutarylated *in vitro* independent of incubation time or glu-CoA concentration, suggesting increases in the stoichiometry rather than increases in the number of glutarylated GDH residues with time or substrate concentration. The low glutarylation stoichiometry of GDH *in vitro* could be confirmed *in vivo* by two-dimensional (2D) gel electrophoresis of mitochondrial extracts

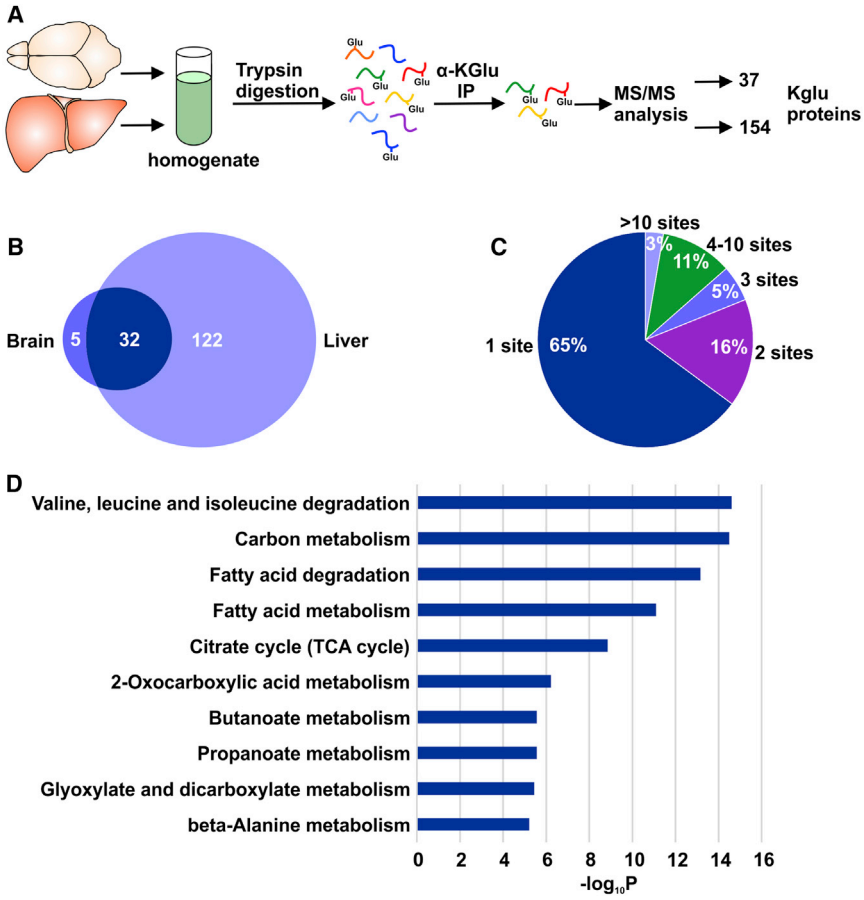

Figure 4. Proteomic Analyses of Kglu Substrates in WT and *Gcdh* KO Mouse Brain and Liver

(A) Experimental approach used to identify glutarylated peptides.

(B) Venn diagram showing the overlap between glutarylated proteins of brain and liver tissue derived from *Gcdh* KO mice.

(C) Distribution of Kglu sites per protein identified by proteomic analysis of brain tissue from *Gcdh* KO mice.

(D) Functional annotation and enrichment analysis of Kglu substrates in brain tissue by analyzing KEGG metabolic pathways.

See also Figure S4, Table 1, and Tables S1 and S2.

of *Gcdh* KO brain and liver followed by anti-Kglu and Gdh western blotting. Three major 55 kDa isoforms (designated 1, 2, and 3) that differ in charge (pI 6.7 to 7.4) were found in *Gcdh* KO extracts with a relative abundance following the order 1 > 2 > 3; this appears to make it the major glutarylated protein in brain tissue (Figure S6A). In WT brain and liver extracts, we observed two Gdh isoforms (1 and 2) only. These surprising data demonstrate that the 11 and 14 different Kglu-modified lysine residues of Gdh identified in brain and liver, respectively, *in vivo* are represented by Gdh isoform 3, suggesting the existence of multiple mono-glutarylated Gdh isoforms modified at various sites simultaneously (Figures S6A and S6B).

The increase in glutarylation stoichiometry *in vitro* was associated with a gradual loss of GDH activity (Figures S5B and S5E) that could be partially reversed by sirtuin 5 treatment (Figure 5B) In contrast, the GDH activity in mitochondrial fractions prepared from brain of 6-week-old WT and *Gcdh* KO mice revealed no significant differences between the genotypes (Figure 5C), which may be explained by the low glutarylation stoichiometry of GDH and the number of mitochondria containing glutarylated GDH.

Previously, we showed that GDH, electron transfer flavoprotein subunit B (ETFB), and dihydrolipoamide S-succinyltransferase (DLST) directly interact with GCDH (Schmiesing et al., 2014). When we incubated GDH that has been glutarylated *in vitro* or not, with purified GCDH coupled to Affi-Gel beads, almost no glutarylated GDH was found to interact with GCDH (Figure 5D). Similarly, purified and *in vitro* glutarylated ETFB, but not DLST, failed to bind to the GCDH matrix (Figures S7A and S7B). Moreover, GCDH, which is not glutarylated in *SIRT5* KO mouse liver *in vivo* (Tan et al., 2014), can be glutarylated *in vitro* (Figure S7C). However, we observed that Kglu modifications of GCDH did not impair the dimerization and binding to non-modified GCDH.

To gain insight into the structural environment of glutarylated lysine residues *in silico*, we performed homology-based three-dimensional structure modeling of mouse Gdh. All lysine residues found to be glutarylated in the mouse Gdh *in vivo*, as well as in the bovine GDH *in vitro*, are conserved. Examination of the glutarylation sites within the three-dimensional (3D) structure of the Gdh hexamer suggest that the glutarylated lysine residues are located at the solvent-exposed surface and not in the hexameric interface of the Gdh monomer (Figure 5E). The *in vivo* glutarylated residues K191 and K352 are close to the NADPH binding site, and K503 and K346 surround the guanosine triphosphate (GTP) binding site (Figure 5F). Similarly, the glutarylated residues K545 and K548 are located close to the ADP effector binding site (Figure 5G). Because the lysine side chains in GDH mostly form salt bridges with the phosphate moieties of substrates and allosteric effectors, it is likely that the negative charge of glutarylated lysines interferes with the formation of salt bridges to the allosteric ligands.

Glutarylation Reduces Ca5b Activity but Not CA4 Activity

Finally, we analyzed carbonic anhydrase 5B (Ca5b), one of the five glutarylated mitochondrial proteins specifically detected in the brain (Table S1). When we glutarylated purified murine carbonic anhydrase 5B (Ca5b) *in vitro* and, as negative control, human carbonic anhydrase 4 (hCA4), only the activity of glutarylated Ca5b, not that of CA4, was strongly reduced (Figures 6A

Table 1. Common Glutarylated Proteins Identified by Mass Spectrometry Analysis of Mitochondrial Extracts from *Gcdh* KO Brain and Liver Tissue, Related to Figure 4, Figure S4, and Table S1

	Protein	Gene	*Gcdh* KO	
			Brain	Liver
1	glutamate dehydrogenase 1	*Glud1*	11[a]	14
2	aconitate hydratase	*Aco2*	6	5
3	trifunctional enzyme subunit alpha	*Hadha*	5	7
4	malate dehydrogenase	*Mdh2*	5	6
5	citrate synthase	*Cs*	4	3
6	trifunctional enzyme subunit beta	*Hadhb*	3	5
7	isocitrate dehydrogenase (NADP)	*Idh2*	3	10
8	4-aminobutyrate aminotransferase	*Abat*	2	2
9	short/branched chain-specific acyl-CoA dehydrogenase	*Acadsb*	2	2
10	ATP synthase subunit beta	*Atp5b*	2	6
11	protein NipSnap homolog 3B	*Nipsnap3b*	2	3
12	succinate dehydrogenase flavoprotein subunit	*Sdha*	2	7
13	acyl-CoA dehydrogenase family member 10	*Acad10*	1	1
14	long-chain-specific acyl-CoA dehydrogenase	*Acadl*	1	2
15	medium-chain-specific acyl-CoA dehydrogenase	*Acadm*	1	2
16	acetyl-CoA acetyltransferase	*Acat1*	1	5
17	acyl-CoA thioesterase 13	*Acot13*	1	1
18	acyl-CoA synthetase family member 2	*Acsf2*	1	1
19	GTP:AMP phosphotransferase AK3	*Ak3*	1	1
20	alpha-aminoadipic semialdehyde dehydrogenase	*Aldh7a1*	1	1
21	ATP synthase subunit O	*Atp5o*	1	6
22	ES1 protein homolog	*D10Jhu81e*	1	1
23	dihydrolipoyl dehydrogenase	*Dld*	1	8
24	delta(3,5)-delta(2,4)-dienoyl-CoA isomerase	*Ech1*	1	1
25	enoyl-CoA hydratase	*Echs1*	1	2
26	enoyl-CoA delta isomerase 2	*Eci2*	1	1
27	aspartate aminotransferase	*Got2*	1	12
28	malonyl-CoA-acyl carrier protein transacylase	*Mcat*	1	1
29	3-mercaptopyruvate sulfurtransferase	*Mpst*	1	1
30	cysteine desulfurase	*Nfs1*	1	1
31	thiosulfate sulfurtransferase	*Tst*	1	3
32	3-ketoacyl-CoA thiolase	*Acaa2*	1	14

[a]Number of glutarylated lysine residues.

and 6B). However, similar to GDH activity in brain, the carbonic anhydrase activity measured in mitochondrial fractions of WT and *Gcdh* KO brains was not significantly changed (Figure 6C), which again might be due to the low percentage of mitochondria containing glutarylated proteins. To analyze the consequences of Kglu on Ca5b activity, we performed *in silico* homology-based modeling of mouse carbonic anhydrase 5b (Ca5b) based on the 70% sequence identity to the human carbonic anhydrase VA (CAVA) structure (PDB: 1KEQ; PMID: 11851394). The glutarylated residue K249 appears to be located at the surface of the protein. At this position, the additional negative charge by glutarylation will most likely impair the surface potential and stability, rather than directly impair the activity of Ca5b, because K249 is too far from the active site (Figure 6D).

These data show that glutarylation of mitochondrial enzymes and co-factors reduces the catalytic activity (GDH and Ca5b), as well as their abilities to interact with constituents of multimeric protein complexes (GCDH and ETFB), most likely due to steric hindrance or negative charges. The low stoichiometry of glutarylation found in a limited number of proteins in glial cells suggests tightly regulated metabolic pathways, which lead to a functional heterogeneity of mitochondria. Whether and how few dysfunctional mitochondria of glial cells containing Kglu-modified proteins impair the homeostasis of *Gcdh*-deficient neuronal cells remains to be studied.

DISCUSSION

The pathophysiological mechanisms leading to the selective bilateral destruction of striatal neurons and subsequent irreversible loss of motor skills in patients with glutaryl-CoA dehydrogenase deficiency are not fully understood. The high level of the toxic metabolites GA and 3-hydroxyglutaric acid (3OH-GA) have been reported to affect NMDA receptors, γ-aminobutyric acid (GABA) synthesis, or mitochondrial energy production (Jafari et al., 2013). However, the significance of these studies is unclear, because they have been performed mainly with cells expressing enzymatically active endogenous GCDH. We showed that both GA and 3OH-GA are substrates for Na^+-coupled dicarboxylate transporters that inhibit the anaplerotic transfer of the TCA cycle intermediate succinate between astrocytes and neurons and subsequently impair the generation of ATP in neuronal cells of *Gcdh* KO mice (Lamp et al., 2011). Secondary Kglu of multiple mitochondrial proteins, which could be shown to inhibit the enzymatic activities of all four investigated enzymes so far, has to be considered as an additional pathogenic mechanism underlying GA1.

Glutarylation Inhibits Activity and Interaction of GDH with Mitochondrial Proteins

The identification of 37 glutarylated mitochondrial proteins in the brain of *Gcdh* KO mice, most of which function in amino acid degradation pathways (valine, leucine, lysine, and tryptophan) and in the TCA cycle (Figure 4D; Tables S1 and S2A), appears to affect general mitochondrial functions. To our surprise, however, the immunogold electron microscopy (EM) analysis of *Gcdh* KO brain sections revealed that only 10% of the mitochondria contain glutarylated proteins. A growing body of evidence has demonstrated that heterogeneity in subcellular distribution, metabolic activity, shape, and density of mitochondria in glial cells is prerequisite for the formation of single functional

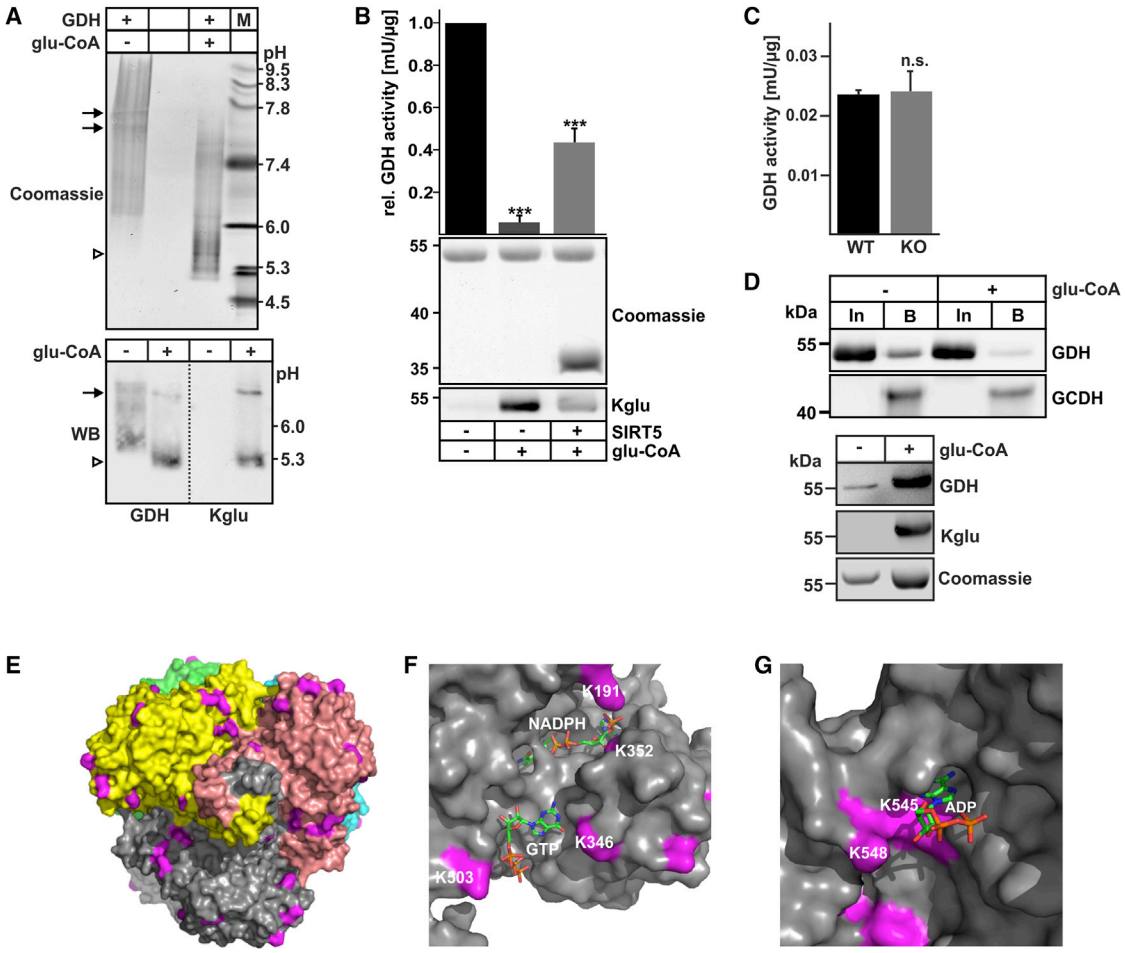

Figure 5. Glutamate Dehydrogenase Is Targeted for Glutarylation

(A) IEF of bovine GDH and *in vitro* glutarylated GDH followed by Coomassie blue staining and anti-Kglu or anti-GDH western blotting. The pH gradient is indicated. Arrows and open arrowheads indicate non-modified and *in vitro* glutarylated GDH, respectively.

(B) Relative GDH activity of untreated purified bovine GDH (control) or glu-CoA-incubated GDH, followed or not by incubation with active SIRT5. The level of protein glutarylation were measured using an anti-Kglu antibody normalized to total GDH protein stained by Coomassie blue. n = 4.

(C) GDH activity in mitochondrial fractions of WT and *Gcdh* KO brain. WT, n = 4; KO, n = 6; n.s., not significant.

(D) Top panel: glutarylation of GDH prevents its capability to interact with GCDH. Purified human GCDH was covalently coupled to Affi-Gel 10 matrix and incubated with non-glutarylated (−) and *in vitro* glutarylated GDH (+). Aliquots of the input (In) and the bound fraction (B) were separated by SDS-PAGE and tested by GDH and GCDH western blotting. Bottom panel: GDH glutarylation was evaluated by GDH and Kglu western blotting and normalized to Coomassie blue-stained GDH protein.

(E) Homology model of mouse Gdh (PDB: 3ETD) as a surface representation (color-coded subunits of the hexamer). Lysine residues identified to be glutarylated in *Gcdh* KO brain *in vivo* are shown in magenta.

(F) Zoom into the surface representation of the Gdh monomer illustrating ligand binding sites. Bound GTP and NADPH are shown as sticks and color coded according to atom type.

(G) Structural analysis of Gdh modeling K545 and K548 and the ADP binding site. Bound ADP is shown as color-coded sticks.

Error bars represent ± SD. ***$p < 0.0001$

See also Figures S5–S7 and Tables S1 and S3.

metabolic units with neuronal cells (Dubinsky, 2009; Oheim et al., 2018). It remains to be studied how glial mitochondria containing glutarylated proteins affect cytosolic microenvironments, such as Ca^{2+} changes, release of reactive oxygen species, ATP generation, and metabolism, particularly that of glutamate, to adapt to metabolic demands of neighboring GCDH-deficient neurons.

Previously, we found that the activity of CPS1, the most highly glutarylated protein in the liver of *Gcdh* KO mice, was reduced in comparison with the non-modified enzyme in WT tissue (Tan et al., 2014). The most abundant glutarylated protein in *Gcdh* KO brain represents the 55 kDa glutamate dehydrogenase (Gdh) (Figure 1A; Figures S5 and S6A; Table S1). Although the enzymatic activity of *in vitro* glutarylated GDH was strongly reduced, the activity was not changed in mitochondrial fractions of *Gcdh* KO brain. The inability to measure significantly reduced GDH activity is most likely because both the stoichiometry of

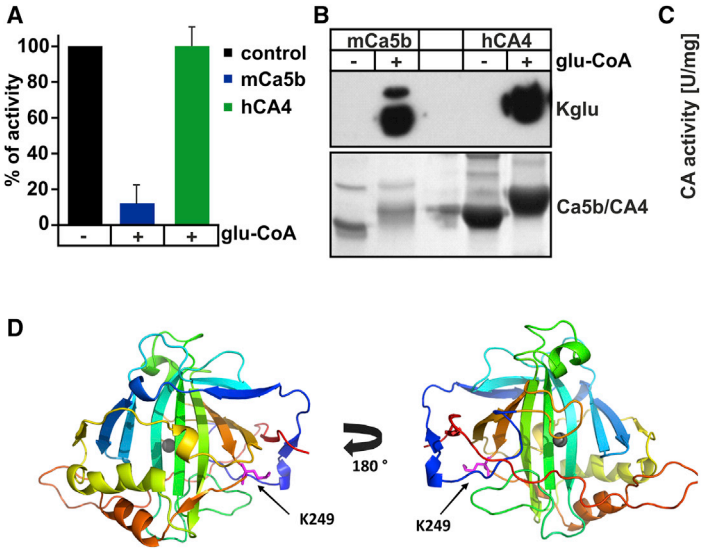

Figure 6. Glutarylation Reduces Carbonic Anhydrase 5B Activity

(A) Enzymatic activity of mouse carbonic anhydrase 5B (Ca5b) and human carbonic anhydrase 4 (CA4), which were incubated in the presence (+) or absence (−) of glu-CoA followed by measurement of enzyme activities expressed as a percentage of non-glutarylated controls. n = 5

(B) Kglu western blot analysis of recombinant Ca5b and CA4 after incubation in the presence (+) or absence (−) of 5 mM glu-CoA for 4 hr. As control, the total amount of Ca5b and CA4 is shown.

(C) Carbonic anhydrase activity in mitochondrial fractions of WT and *Gcdh* KO brain. n = 6 of each genotype; n.s., not significant.

(D) Homology model of glutarylated Ca5b rainbow color coded from blue (N term) to red (C term). Glutarylated K249 (arrow) is shown in magenta as sticks, and Zn^{2+} is shown in the active site as a gray ball. The homology model was generated using the 70% identical murine CAVA structure (PDB: 1KEQ) as a template.

Error bars represent ± SD.

Related to Table S1.

GDH glutarylation and the number of mitochondria containing glutarylated proteins are too low to make its presence detectable in total brain extracts.

GDH is a homohexameric enzyme that is regulated by various allosteric effectors, e.g., GTP as a negative effector and ADP and L-leucine as positive effectors. GDH catalyzes the reversible oxidative deamination of glutamate to α-ketoglutarate and plays a central role in nitrogen glutamate metabolism, cellular energy homeostasis, and cell signaling (Plaitakis et al., 2017). *In silico* homology-based 3D structure modeling of mouse Gdh revealed that the lysines identified to be glutarylated *in vivo* in *Gcdh* KO brain may be responsible for perturbation in the allosteric effector and NADPH binding, rather than intersubunit interactions (Figures 5E–5G). Furthermore, we have previously demonstrated that GDH interacts with GCDH (Schmiesing et al., 2014), and we showed here that this interaction is strongly blocked by glutarylation (Figure 5D), most likely by increasing the negative surface charges of GDH.

In agreement with our *in vitro* GDH glutarylation experiments (Figure S5; Table S3), it has been shown that various reactive acyl-CoA species, including glu-CoA, generate the lysine modifications of proteins in a non-enzymatic manner (Wagner et al., 2017). In addition to the dependency of lysine acylation on the abundance of the protein (Weinert et al., 2013), the non-enzymatic transfer of glutaryl residues may also explain the differential extent of protein glutarylation in various tissues of *Gcdh* KO mice. The steady-state concentration of non-metabolized glutaryl-CoA is several fold higher in liver and kidney than in brain of *Gcdh* KO mice (Figure 1A). Moreover, although the concentrations of cytotoxic GA and 3OHGA increase upon induced encephalopathic crisis (Strauss et al., 2003; Zinnanti et al., 2006) the intensity and pattern of glutarylated proteins in *Gcdh* KO brain and liver extracts are unchanged (Figure 2A; Figure S1B), suggesting the existence of regulatory mechanisms adjusting the glutaryl-CoA level independent of catabolic conditions.

Neither immunohistochemistry nor immunogold EM analyses on brain sections provided evidence for the localization of glutarylated proteins in mitochondria of synaptic boutons or in perikarya of neuronal cells, rather than their exclusive accumulation in mitochondria of glial cells (Figures 3A–3D). These findings are in agreement with the predominant localization of GDH in astrocytes and Bergmann glia (Aoki et al., 1987; Plaitakis et al., 2017) that positively correlates with terminal fields of glutamatergic transmission and expression of glutamate transporters GLT1 and GLAST (Rothstein et al., 1994) required for clearance of synaptically released glutamate to avoid excitotoxicity. Once internalized into astrocytes, glutamate is either transformed into glutamine and subsequently transported to neurons or transformed back into glutamate and packed into synaptic vesicles as a neurotransmitter.

It remains to be examined whether inhibitory effects of glutarylation on catalytic activity and/or the loss of effector-mediated allosteric regulation of GDH activity in astrocytic mitochondria are sufficient to significantly increase glutamate levels contributing subsequently to brain damage due to excitotoxicity (Facheris et al., 2004). This might be potentiated by the strongly elevated level of the neurotoxic GA1 metabolite GA, exhibiting structural similarities with glutamate (Goodman and Frerman, 2001), which blocks the astrocytic efflux and neuronal uptake of the TCA cycle intermediates for ATP generation (Lamp et al., 2011). Finally, GDH has been reported to be part of supramolecular structures (metabolons) with the 2-oxoglutarate dehydrogenase complex, branched-chain amino acid metabolic enzymes, Got2, or GCDH (Hutson et al., 2011; Schmiesing et al., 2014; Zhang et al., 2006). Therefore, we hypothesized that Kglu of GDH may also impair metabolon functions and energy homeostasis; future studies will be directed at testing this hypothesis.

Glutarylation Controls Carbonic Anhydrase 5B Activity

We next examined carbonic anhydrase 5b (Ca5b), which is one of the five mitochondrial proteins that is uniquely glutarylated in

the brain of *Gcdh* KO mice at K249. Ca5b belongs to a family of 13 zinc metalloenzymes that catalyze the reversible hydration of CO_2 in the reaction of $CO_2 + H_2O \Leftrightarrow HCO_3^- + H^+$ that plays an important role in regulation of the acid-base balance, bone resorption, and several metabolic pathways (Sly and Hu, 1995). We could show that *in vitro* glutarylation of Ca5b results in loss of activity, whereas similarly to GDH, the activity of Ca5b in mitochondrial fractions of *Gcdh* KO mouse brain is not significantly impaired (Figure 6C). *In silico* modeling of glutarylated Ca5b demonstrated that the distance of the glutarylated K249 residue to the catalytic center excludes a direct effect on activity (Figure 6D), rather than loss of protein-protein interactions or reduced stability of the enzyme. Preliminary data suggest that CA5A could associate with several mouse mitochondrial proteins, including succinate dehydrogenase, pyruvate decarboxylase, malate dehydrogenase, aconitate dehydrogenase and catalase, and 2-oxoglutarate dehydrogenase. However, the association of Ca5b with mitochondrial proteins remains to be examined. With analogy to human CA2 and human CA5A, the V206-K239 segment of the carbonic anhydrases is structurally important (Shah et al., 2000). Two mutations, an S233P missense mutation and a deletion of residues 207–258, have been identified in the *CA5A* gene of two families with infantile hyperammonemic encephalopathy, which affect the V206-K239 segment and lead to instability and loss of the CA5A protein, respectively (van Karnebeek et al., 2014). Therefore, it is likely that glutarylation of K249 close to the V206-K239 segment results in a secondary loss of Ca5b enzymatic activity due to decreased stability. Because mitochondria are impermeable to HCO_3^-, Ca5b is pivotal in providing HCO_3^- for the activity of four mitochondrial enzymes: carbamoyl-phosphate synthetase 1, pyruvate carboxylase, propionyl-CoA carboxylase, and methylcrotonyl-CoA carboxylase (van Karnebeek et al., 2014). The significance of glutarylated Ca5b for the activity of these enzymes needs to be evaluated.

Altogether, the findings presented here provide evidence that Kglu of mitochondrial enzymes impairs their activity, protein-protein interactions, and/or stability. These functionally affected glutarylated proteins and the highly elevated metabolites GA and 3OHGA during the metabolic crisis in patients and mice may subsequently change the metabolism of glial cells, in particular the anaplerotic transfer of TCA cycle intermediates and glutamine to neurons required for the generation of both ATP and neurotransmitters. The data support a mechanistic concept of mitochondrial heterogeneity and vulnerability in glial cells initiated by glutarylation of mitochondrial proteins to response to metabolic demands of neighboring neuronal cells in the pathogenesis of GA1 disease.

EXPERIMENTAL PROCEDURES

Additional details can be found in the Supplemental Experimental Procedures.

Electron Microscopy

For electron microscopy, 100-μm-thick vibratome sections of the cerebellum were prepared. For post-embedding immunogold labeling, ultrathin sections (70 nm) were prepared from cryoprotected cerebellar and liver tissue (2.3 M sucrose) and labeled as described previously (Slot and Geuze, 2007).

Immunoprecipitation of Kglu Peptides

Glutarylated peptides from mouse brain or liver were immunoprecipitated according to Chen et al. (2013) with slight modifications, using frozen mouse tissue instead of cultured cell material. The tissue was weighed and homogenized by a dounce homogenizer in 5-fold volume of lysis buffer (0.1 M NaCl, 0.5 mM EDTA, 20 mM Tris-HCl [pH 8.0], 0.5% Nonidet P-40 [NETN]), incubated for 1 hr on ice, treated by ultrasonification, and centrifuged at 16,000 × *g* for 15 min at 4°C. The pellet was resuspended in NETN buffer, and the procedure repeated. Both supernatants were pooled and used for trichloroacetic acid precipitation and Kglu immunoprecipitation as described. For alkylation of free sulfhydryl groups on cysteine residues, 1% acrylamide was used instead of iodoacetamide to avoid artificial lysine modifications.

Liquid Chromatography-MS Measurements

Peptides were redissolved in 8 μL of 0.1% trifluoroacetic acid (TFA) (v/v), and 2.5 μL were injected onto a C18 trap column (20 mm length, 100 μm inner diameter, ReproSil-Pur 120 C18-AQ, 5 μm, Dr. Maisch GmbH, Ammerbuch-Entringen, Germany) made in house. Peptides were separated on a C18 analytical column (200 mm length, 75 μm inner diameter, ReproSil-Pur 120 C18-AQ, 3 μm). Solvent A was 0.1% formic acid, a linear gradient of 3% to 55% solvent B (80% acetonitrile and 0.1% formic acid) at 350 nL/min. The nanoHPLC was coupled online to an LTQ Orbitrap Velos mass spectrometer (Thermo Fisher Scientific, Bremen, Germany). Ions between 330 and 1,700 m/z were scanned in the Orbitrap detector with a resolution of 30,000. Technical replicate 1 was acquired with a gradient length of 90 min and collision-induced dissociation (CID) of the 25 most intense precursor ions (intensity threshold of 5,000, charge $\geq$ 2, 1.5 Da isolation width, 35% normalized energy, and fragment analysis in the linear ion trap). A 200-min gradient was used for technical replicate 2. Fragmentation of the top 20 ions was done with higher-energy CID (HCD; 42% normalized energy and fragment detection in the Orbitrap). Ions were excluded from repeat analysis for 15 s.

MS Data Analysis

Raw data processing and analysis of database searches were performed with Proteome Discoverer v.2.1.1.21 (Thermo Fisher Scientific). Peptide identification was done with an in-house Mascot server v.2.5.1 (Matrix Science, London, UK). Tandem MS (MS2) data were searched against murine sequences from SwissProt (release 2017_01). Precursor Ion m/z tolerance was 5 ppm to exclude false annotations of di-glycine remnants from ubiquitinated proteins (11 mDa mass difference). Fragment ion tolerance was 0.5 Da (CID) or 0.02 Da (HCD). Tryptic peptides with up to two missed cleavage were searched. Propionamide (Cys) was set as a static modification. Oxidation (Met), acetylation (protein N terminus), and glutarylation (C5H6O3: 114.03169 Da on Lys) were allowed as dynamic modifications. Mascot results were assigned posterior error probabilities (PEPs) by the percolator algorithm (Käll et al., 2008) v.2.05 as implemented in Proteome Discoverer. Spectra with identifications with PEP > 0.01 were sent to a second round of database search with semitryptic enzyme specificity (one missed cleavage allowed). Proteins were included if at least two peptides were identified with <1% FDR after built-in Ovality algorithm re-assessment.

IEF Gel Electrophoresis

For isoelectrical focusing (IEF) gel electrophoresis, Criterion IEF Precast Gels (pH 3–10) were used, following the manual instructions. Purified bovine glutamate dehydrogenase (20 μg for Coomassie staining and 100 ng for western blot analysis) was mixed 1:1 with IEF sample buffer and separated using a three-step program: 100 V for 1 hr, 250 V for 1 hr, and 500 V for 30 min.

In Vitro Glutarylation of GDH and Carbonic Anhydrase

Purified bovine glutamate dehydrogenase (GDH), recombinant DLST, the electron transfer flavoprotein subunit B (ETFB), glutaryl-CoA dehydrogenase (GCDH) (Schmiesing et al., 2014), recombinant murine carbonic anhydrase 5B (Ca5b), and human carbonic anhydrase 4 (CA4) (Hu et al., 1995; Waheed et al., 1997) at 1 mg/mL in glutarylation buffer (50 mM HEPES [pH 8.0], 150 mM NaCl, and protease inhibitors) were mixed with 5 mM glutaryl-CoA to form glutaryl-GDH (GDH-glu), glutaryl-DLST, glutaryl-ETFB, glutaryl-Ca5b, and glutaryl-CA4, respectively. The reactions were incubated in an

Eppendorf Thermomixer for 4 hr at 37°C at 400 rpm. To minimize condensation, samples were briefly centrifuged every hour during incubation.

In Vitro Deglutarylation of GDH by SIRT5

For the deglutarylation assay, the glutarylated GDH sample was dialyzed using an Amicon Ultra-Centrifugal Filter with Ultracel-10 membrane, following the manufacturer's instructions. The concentrated sample was reconstituted in SIRT5 assay buffer (50 mM Tris-HCl [pH 8.0], 1 mM $MgCl_2$, 137 mM NaCl, 2.7 mM KCl, and 1 mM NAD^+). Afterward, *in vitro* deglutarylation reactions were performed in a final volume of 50 μL. Then, 3 μg glutarylated GDH were incubated with or without 10 μg SIRT5 in SIRT5 assay buffer for 1 hr at 37°C. Reactions were stopped by adding SDS sample buffer or GDH assay buffer.

GDH Activity Assay

GDH activity was determined by a coupled enzyme assay from Sigma-Aldrich. See Supplemental Experimental Procedures for details.

Carbonic Anhydrase Activity Assay

Ca5b and CA4 enzyme activities were determined using Maren's procedure (Maren, 1960) as described previously (Sundaram et al., 1986).

Animal Experiments

Animal studies were performed in accordance with institutional guidelines. See Supplemental Experimental Procedures for details.

DATA AND SOFTWARE AVAILABILITY

The accession number for the MS proteomics data reported in this paper is PRIDE: PXD007881.

SUPPLEMENTAL INFORMATION

Supplemental information includes Supplemental Experimental Procedures, seven figures, and three tables and can be found with this article online at https://doi.org/10.1016/j.celrep.2018.08.014.

ACKNOWLEDGMENTS

This work was supported by Deutsche Forschungsgemeinschaft (DFG) (MU1778/3-2 to J.S. and C.M. and GRK1459 to A.-C.D., S.S., and T.B.). The authors thank Dr. Michael Woontner and Professor Stephen I. Goodman (University of Colorado Health Sciences Center, Denver) for providing the rabbit anti-human GCDH antibody and are grateful to the Microscopy Imaging Facility of the University Medical Center Hamburg-Eppendorf for support.

AUTHOR CONTRIBUTIONS

J.S., S.S., A.-C.D., M.S., G.M.-F., M.T., M.S., C.M.-S., F.K.-N., and A.W. conceived and performed all experiments. J.S., C.M., V.G., and T.B. supervised the work. H.T. performed *in silico* 3D modeling analysis. C.M., V.G., W.S.S., and T.B. acquired funding. J.S. and T.B. designed the overall study and wrote the manuscript. All authors discussed the results and made substantial contributions to the manuscript.

DECLARATION OF INTERESTS

The authors declare no competing interests.

Received: November 27, 2017
Revised: June 20, 2018
Accepted: August 6, 2018
Published: September 11, 2018

REFERENCES

Aoki, C., Milner, T.A., Sheu, K.F., Blass, J.P., and Pickel, V.M. (1987). Regional distribution of astrocytes with intense immunoreactivity for glutamate dehydrogenase in rat brain: implications for neuron-glia interactions in glutamate transmission. J. Neurosci. *7*, 2214–2231.

Chen, Y., Colak, G., and Zhao, Y. (2013). SILAC-based quantification of Sirt1-responsive lysine acetylome. Methods Mol. Biol. *1077*, 105–120.

Dubinsky, J.M. (2009). Heterogeneity of nervous system mitochondria: location, location, location!. Exp. Neurol. *218*, 293–307.

Facheris, M., Beretta, S., and Ferrarese, C. (2004). Peripheral markers of oxidative stress and excitotoxicity in neurodegenerative disorders: tools for diagnosis and therapy? J. Alzheimers Dis. *6*, 177–184.

Goodman, S.I., and Frerman, F.E. (2001). Organic acidemias due to defects in lysine oxidation: 2-ketoadipic acidemia and glutaric acidemia. In The Metabolic and Molecular Bases of Inherited Disease, C.R. Scriver, A.L. Beaudet, W.S. Sly, D. Valle, B. Childs, K.W. Kinzler, and B. Vogelstein, eds. (McGraw-Hill), pp. 2195–2204.

Goodman, S.I., Kratz, L.E., DiGiulio, K.A., Biery, B.J., Goodman, K.E., Isaya, G., and Frerman, F.E. (1995). Cloning of glutaryl-CoA dehydrogenase cDNA, and expression of wild type and mutant enzymes in *Escherichia coli*. Hum. Mol. Genet. *4*, 1493–1498.

Hu, P.Y., Waheed, A., and Sly, W.S. (1995). Partial rescue of human carbonic anhydrase II frameshift mutation by ribosomal frameshift. Proc. Natl. Acad. Sci. USA *92*, 2136–2140.

Hutson, S.M., Islam, M.M., and Zaganas, I. (2011). Interaction between glutamate dehydrogenase (GDH) and L-leucine catabolic enzymes: intersecting metabolic pathways. Neurochem. Int. *59*, 518–524.

Jafari, P., Braissant, O., Zavadakova, P., Henry, H., Bonafé, L., and Ballhausen, D. (2013). Ammonium accumulation and cell death in a rat 3D brain cell model of glutaric aciduria type I. PLoS ONE *8*, e53735.

Käll, L., Storey, J.D., MacCoss, M.J., and Noble, W.S. (2008). Assigning significance to peptides identified by tandem mass spectrometry using decoy databases. J. Proteome Res. *7*, 29–34.

Keyser, B., Glatzel, M., Stellmer, F., Kortmann, B., Lukacs, Z., Kölker, S., Sauer, S.W., Muschol, N., Herdering, W., Thiem, J., et al. (2008). Transport and distribution of 3-hydroxyglutaric acid before and during induced encephalopathic crises in a mouse model of glutaric aciduria type 1. Biochim. Biophys. Acta *1782*, 385–390.

Koeller, D.M., Woontner, M., Crnic, L.S., Kleinschmidt-DeMasters, B., Stephens, J., Hunt, E.L., and Goodman, S.I. (2002). Biochemical, pathologic and behavioral analysis of a mouse model of glutaric acidemia type I. Hum. Mol. Genet. *11*, 347–357.

Kölker, S., Valayannopoulos, V., Burlina, A.B., Sykut-Cegielska, J., Wijburg, F.A., Teles, E.L., Zeman, J., Dionisi-Vici, C., Barić, I., Karall, D., et al. (2015). The phenotypic spectrum of organic acidurias and urea cycle disorders. Part 2: the evolving clinical phenotype. J. Inherit. Metab. Dis. *38*, 1059–1074.

Lamp, J., Keyser, B., Koeller, D.M., Ullrich, K., Braulke, T., and Mühlhausen, C. (2011). Glutaric aciduria type 1 metabolites impair the succinate transport from astrocytic to neuronal cells. J. Biol. Chem. *286*, 17777–17784.

Maren, T.H. (1960). A simplified micromethod for the determination of carbonic anhydrase and its inhibitors. J. Pharmacol. Exp. Ther. *130*, 26–29.

Oheim, M., Schmidt, E., and Hirrlinger, J. (2018). Local energy on demand: Are "spontaneous" astrocytic Ca^{2+}-microdomains the regulatory unit for astrocyte-neuron metabolic cooperation? Brain Res. Bull. *136*, 54–64.

Plaitakis, A., Kalef-Ezra, E., Kotzamani, D., Zaganas, I., and Spanaki, C. (2017). The glutamate dehydrogenase pathway and its roles in cell and tissue biology in health and disease. Biology (Basel) *6*, E11.

Rothstein, J.D., Martin, L., Levey, A.I., Dykes-Hoberg, M., Jin, L., Wu, D., Nash, N., and Kuncl, R.W. (1994). Localization of neuronal and glial glutamate transporters. Neuron *13*, 713–725.

Schmiesing, J., Schlüter, H., Ullrich, K., Braulke, T., and Mühlhausen, C. (2014). Interaction of glutaric aciduria type 1-related glutaryl-CoA dehydrogenase with mitochondrial matrix proteins. PLoS ONE *9*, e87715.

Shah, G.N., Hewett-Emmett, D., Grubb, J.H., Migas, M.C., Fleming, R.E., Waheed, A., and Sly, W.S. (2000). Mitochondrial carbonic anhydrase CA VB: differences in tissue distribution and pattern of evolution from those of CA VA suggest distinct physiological roles. Proc. Natl. Acad. Sci. USA *97*, 1677–1682.

Slot, J.W., and Geuze, H.J. (2007). Cryosectioning and immunolabeling. Nat. Protoc. *2*, 2480–2491.

Sly, W.S., and Hu, P.Y. (1995). Human carbonic anhydrases and carbonic anhydrase deficiencies. Annu. Rev. Biochem. *64*, 375–401.

Strauss, K.A., Puffenberger, E.G., Robinson, D.L., and Morton, D.H. (2003). Type I glutaric aciduria, part 1: natural history of 77 patients. Am. J. Med. Genet. C. Semin. Med. Genet. *121C*, 38–52.

Sundaram, V., Rumbolo, P., Grubb, J., Strisciuglio, P., and Sly, W.S. (1986). Carbonic anhydrase II deficiency: diagnosis and carrier detection using differential enzyme inhibition and inactivation. Am. J. Hum. Genet. *38*, 125–136.

Tan, M., Peng, C., Anderson, K.A., Chhoy, P., Xie, Z., Dai, L., Park, J., Chen, Y., Huang, H., Zhang, Y., et al. (2014). Lysine glutarylation is a protein posttranslational modification regulated by SIRT5. Cell Metab. *19*, 605–617.

Thies, B., Meyer-Schwesinger, C., Lamp, J., Schweizer, M., Koeller, D.M., Ullrich, K., Braulke, T., and Mühlhausen, C. (2013). Acute renal proximal tubule alterations during induced metabolic crises in a mouse model of glutaric aciduria type 1. Biochim. Biophys. Acta *1832*, 1463–1472.

van Karnebeek, C.D., Sly, W.S., Ross, C.J., Salvarinova, R., Yaplito-Lee, J., Santra, S., Shyr, C., Horvath, G.A., Eydoux, P., Lehman, A.M., et al. (2014). Mitochondrial carbonic anhydrase VA deficiency resulting from CA5A alterations presents with hyperammonemia in early childhood. Am. J. Hum. Genet. *94*, 453–461.

Vizcaíno, J.A., Deutsch, E.W., Wang, R., Csordas, A., Reisinger, F., Ríos, D., Dianes, J.A., Sun, Z., Farrah, T., Bandeira, N., et al. (2014). ProteomeXchange provides globally coordinated proteomics data submission and dissemination. Nat. Biotechnol. *32*, 223–226.

Wagner, G.R., Bhatt, D.P., O'Connell, T.M., Thompson, J.W., Dubois, L.G., Backos, D.S., Yang, H., Mitchell, G.A., Ilkayeva, O.R., Stevens, R.D., et al. (2017). A class of reactive acyl-CoA species reveals the non-enzymatic origins of protein acylation. Cell Metab. *25*, 823–837.e8.

Waheed, A., Pham, T., Won, M., Okuyama, T., and Sly, W.S. (1997). Human carbonic anhydrase IV: *in vitro* activation and purification of disulfide-bonded enzyme following expression in *Escherichia coli*. Protein Expr. Purif. *9*, 279–287.

Weinert, B.T., Schölz, C., Wagner, S.A., Iesmantavicius, V., Su, D., Daniel, J.A., and Choudhary, C. (2013). Lysine succinylation is a frequently occurring modification in prokaryotes and eukaryotes and extensively overlaps with acetylation. Cell Rep. *4*, 842–851.

Zhang, L., Cooper, A.J., Krasnikov, B.F., Xu, H., Bubber, P., Pinto, J.T., Gibson, G.E., and Hanigan, M.H. (2006). Cisplatin-induced toxicity is associated with platinum deposition in mouse kidney mitochondria *in vivo* and with selective inactivation of the alpha-ketoglutarate dehydrogenase complex in LLC-PK1 cells. Biochemistry *45*, 8959–8971.

Zinnanti, W.J., Lazovic, J., Wolpert, E.B., Antonetti, D.A., Smith, M.B., Connor, J.R., Woontner, M., Goodman, S.I., and Cheng, K.C. (2006). A diet-induced mouse model for glutaric aciduria type I. Brain *129*, 899–910.

Cell Reports, Volume *24*

Supplemental Information

Disease-Linked Glutarylation Impairs Function and Interactions of Mitochondrial Proteins and Contributes to Mitochondrial Heterogeneity

Jessica Schmiesing, Stephan Storch, Ann-Cathrin Dörfler, Michaela Schweizer, Georgia Makrypidi-Fraune, Melanie Thelen, Marc Sylvester, Volkmar Gieselmann, Catherine Meyer-Schwesinger, Friedrich Koch-Nolte, Henning Tidow, Chris Mühlhausen, Abdul Waheed, William S. Sly, and Thomas Braulke

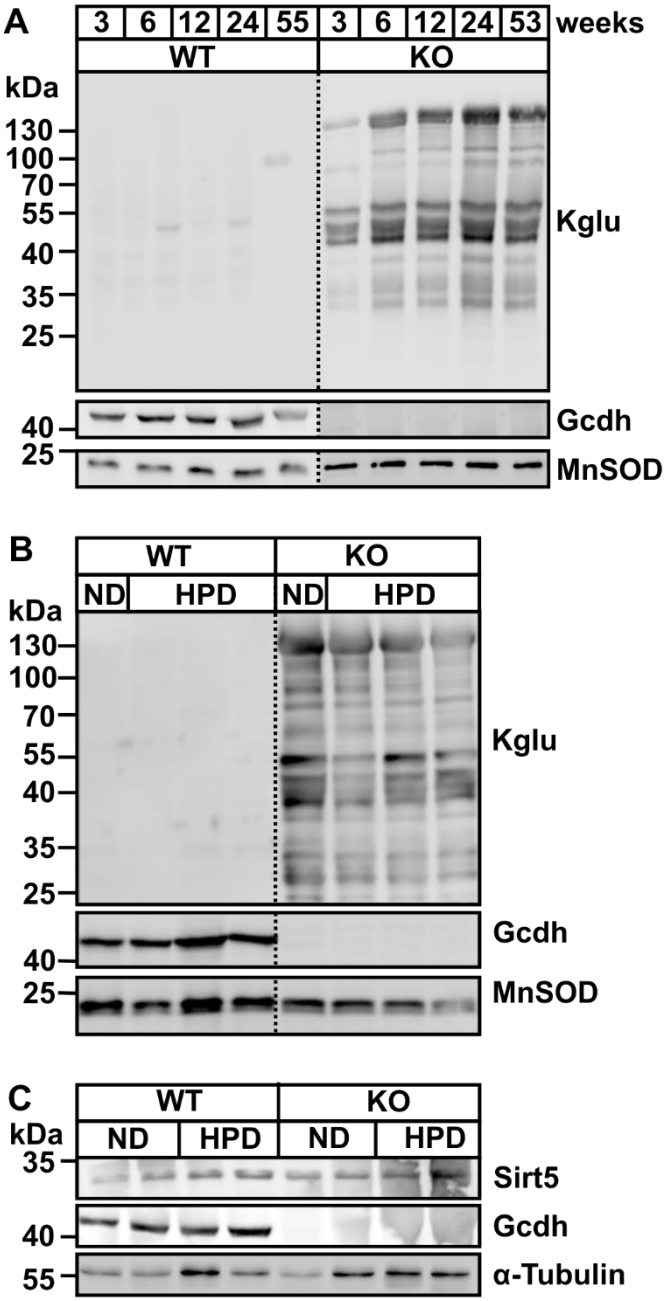

Figure S1. High protein diet-induced metabolic crisis fails to increase the extent of protein glutarylation in liver of wild-type and *Gcdh* KO mice. Related to Figure 1 and 2

(A) Age-dependency of protein glutarylation in hepatic mitochondrial extracts of WT and *Gcdh* KO mice. (B) Kglu immunoblotting of extracts of hepatic mitochondrial fractions of 6 week-old WT and *Gcdh* KO mice. The mice were fed with normal diet (ND) or high protein diet (HPD) for four days. Gcdh and MnSOD expression were used as control. (C**)** Sirt5 western blot analysis of liver mitochondrial extracts prepared from WT and *Gcdh* KO mice under ND or HPD. Gcdh and α-tubulin expression were used as controls.

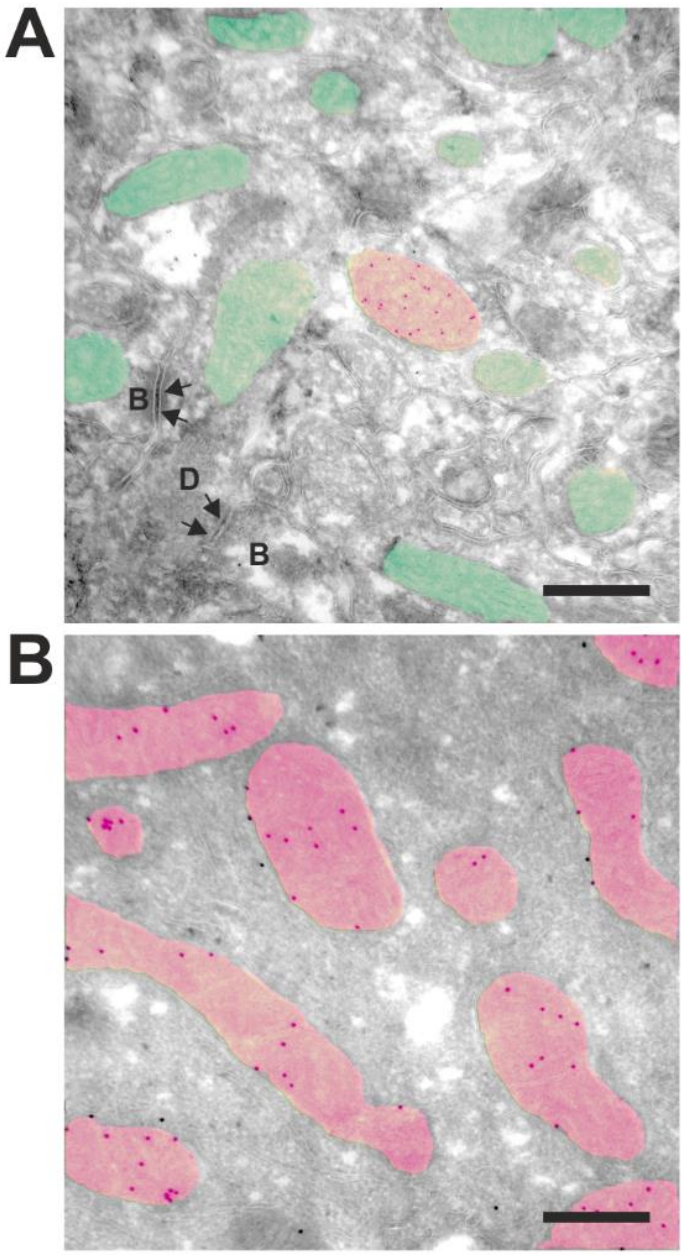

Figure S2. Distribution of Kglu-modified proteins in mitochondria of brain and liver sections *Gcdh* KO mice. Related to Figure 3 and Figure S3

(A) Representative ultrathin cryo-sections of *Gcdh* KO mouse brain were incubated with anti-Kglu antibodies and protein A gold (10 nm) secondary antibodies. Arrows indicate the synaptic contacts between the presynaptic bouton (B) and dendrite (D). Mitochondria containing Kglu-modified proteins (light red) or not (light green) are shown. Scale bar: 500 nm comprehensive view. (B) Kglu-immuno-gold (15 nm) labeled mitochondria (light red) in ultrathin sections of *Gcdh* KO mouse liver. Scale bar: 500 nm comprehensive view.

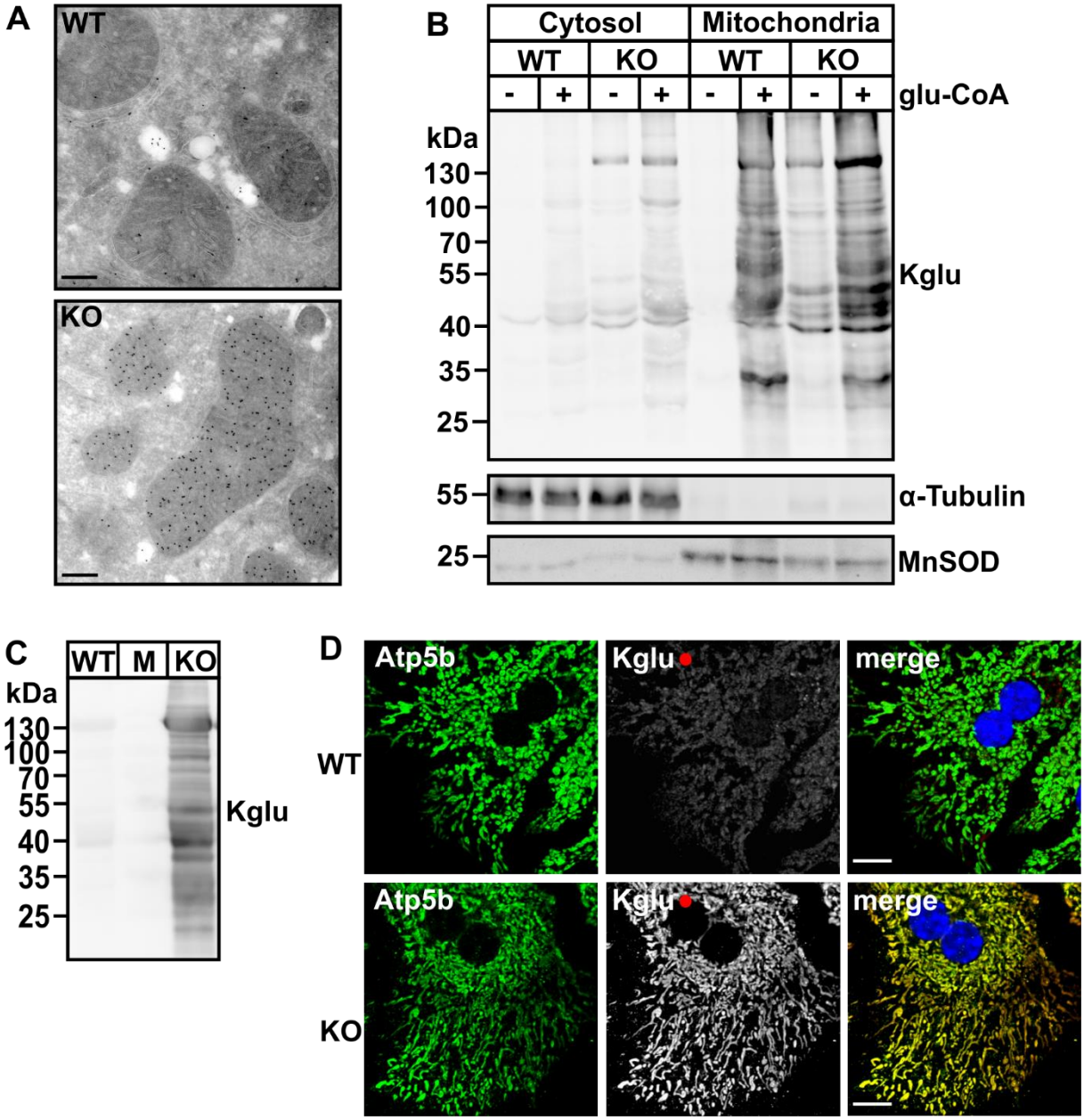

Figure S3. Mitochondrial localization of glutarylated proteins in liver and cultured hepatocytes of WT and *Gcdh* KO mice. Related to Figure 3 and Figure S2

(A) Ultrathin sections of hepatocytes prepared by cryosectioning of liver tissue from WT and *Gcdh* KO mice and anti-KGlu immunogold labeling. Scale bar, 250 nm. (B) *In vitro* glutarylation of cytosolic and mitochondrial fractions isolated from liver of WT and *Gcdh* KO mice. Protein glutarylation was visualized by Kglu western blotting. α-Tubulin and MnSOD expression were analyzed as cytosolic and mitochondrial marker proteins, respectively. (C) Kglu western blot analysis of cultured hepatocytes isolated from WT and *Gcdh* KO mice. M, lane with molecular mass marker proteins. (D) Immunofluorescence images of cultured hepatocytes isolated from WT and *Gcdh KO* mice grown on coverslips, co-stained for the mitochondrial marker protein Atp5b (green) and glutarylated proteins (Kglu, red), followed by confocal laser scan microscopy. Scale bar, 10 µm.

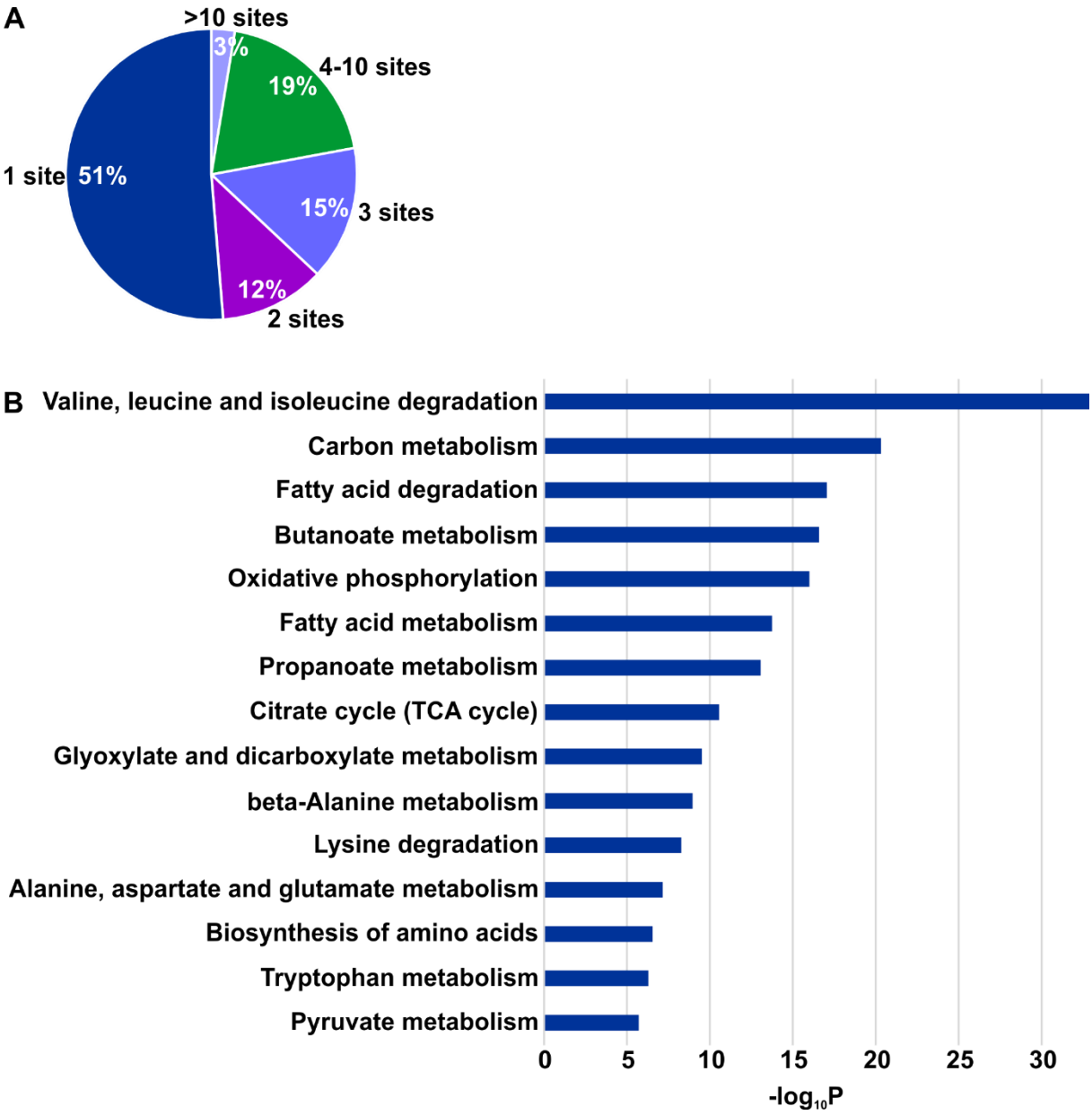

Figure S4. Variable number of glutarylated residues and functional enrichment analysis of Kglu substrates in *Gcdh* KO mouse liver. Related to Figure 4 and Tables S1 and S2

(A) Distribution of Kglu sites per protein identified by proteomic analysis of liver tissue from *Gcdh* KO mouse. (B) Functional annotation and enrichment analysis of Kglu substrates in liver tissue by analyzing KEGG metabolic pathways.

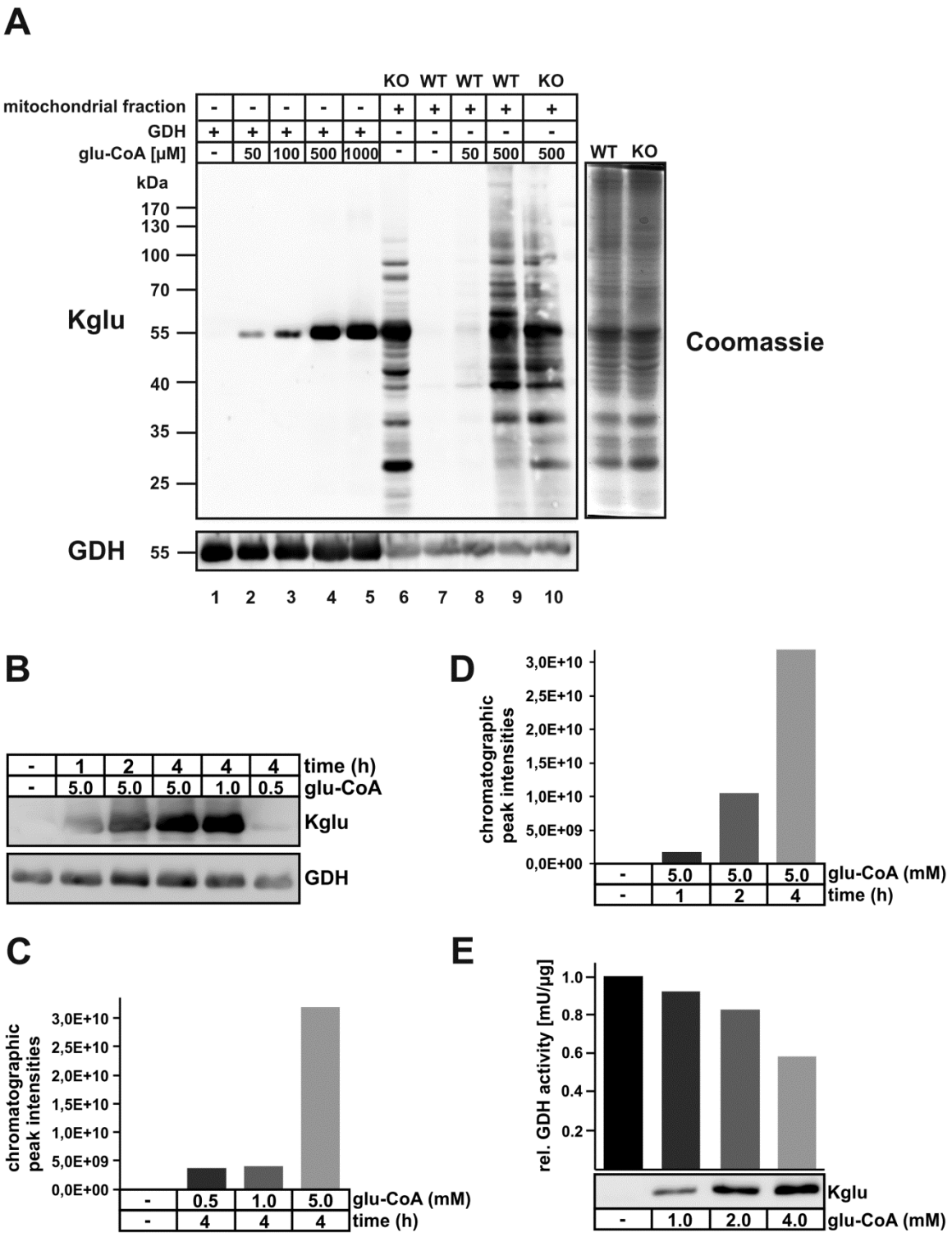

Figure S5. *in vitro* Glutarylation of GDH and effect on GDH activity. Related to Figure 5 and Tables S1 and S3

(A) Purified bovine GDH (200 ng) and brain mitochondrial fractions (75 µg protein) from WT and *Gcdh* KO mice were incubated in the absence (-) or presence of increasing concentrations of glu-CoA for 4 h at 37°C.

Protein glutarylation was visualized by Kglu western blotting. GDH western blotting and Coomassie blue staining were used for loading control. The positions of the molecular mass markers are indicated. (B) Kglu-specific western blot analysis of *in vitro* modified bovine GDH in dependency of incubation time- and glu-CoA-concentration. Samples were also used for MS analysis. (C) Time-dependent progression of *in vitro* glutarylated GDH analyzed by mass spectrometry. Peak areas of extracted ion chromatograms of all Kglu-peptides of one sample were summed up. (D) Glu-CoA-dependent progression of *in vitro* glutarylated GDH analyzed by mass spectrometry. Peak areas of extracted ion chromatograms of all Kglu-peptides of one sample were summed up. (E) Relative protein activity of purified bovine GDH measured after incubation in the absence (-) or presence of 1, 2 or 4 mM glu-CoA for 4h. The level of protein glutarylation was determined by Kglu western blotting.

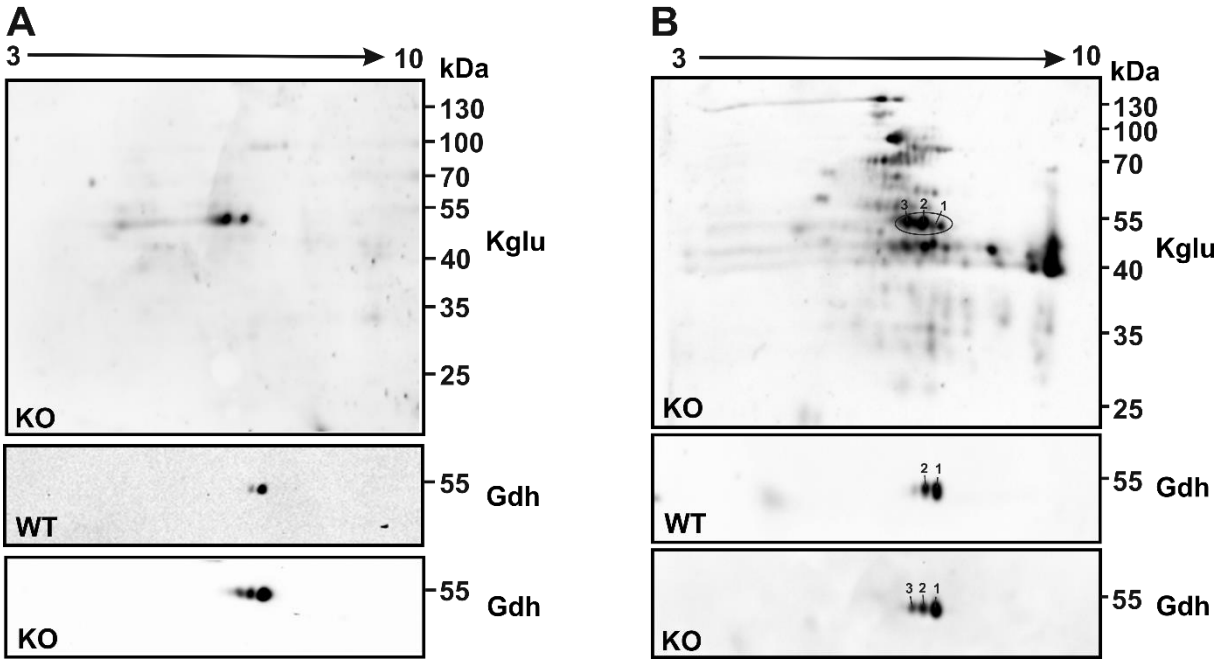

Figure S6. Low glutarylation stoichiometry of Gdh in *Gcdh* KO tissues. Related to Figure 5, Figure S7 and Table S1

(A) Mitochondrial extracts from WT and *Gcdh* KO mouse brain and (B) liver were separated by isoelectric focusing (pH gradient 3 to 10) followed by SDS-PAGE and anti-Kglu and anti-GDH western blotting. The three Gdh isoforms are indicated.

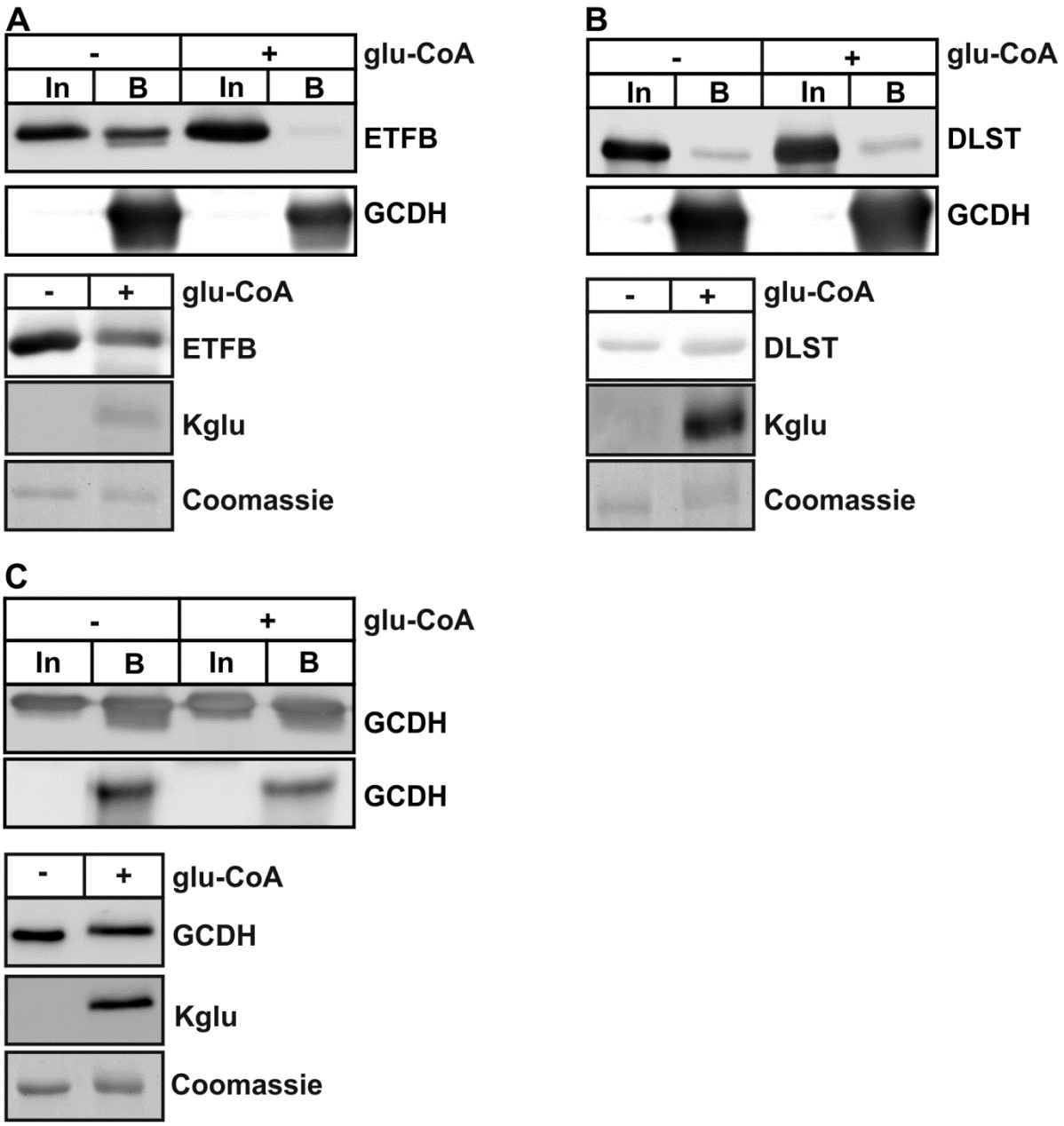

Figure S7. Glutarylation impairs GDH- and ETFB-protein interactions. Related to Figure 5 and Table S3

(A) Top panel: Glutarylated ETFB (+ glu-CoA) fails to bind to GCDH. In, input; B, bound fraction. Bottom panel: ETFB and Kglu western blotting, and Coomassie blue staining. Of note, Kglu residues appear to impair anti-ETFB antibody recognition. (B) Top panel, DLST and GCDH western blotting show that binding of glutarylated DLST (+ glu-CoA) to GCDH is not affected. Bottom panel: Level of DLST glutarylation analyzed by western blotting, and Coomassie blue staining. (C) Top panel, GCDH western blotting show that dimerization of glutarylated GCDH (+ glu-CoA) with GCDH is not affected. Bottom panel: Level of GCDH glutarylation analyzed by western blotting, and Coomassie blue staining

Table S1. Proteomic analysis of Kglu substrates in *Gcdh* KO mouse brain and liver[1]. Related to Figure 4, Figure 5, Table S2, and Table S3.

Protein	Gene	Brain	Liver
Glutamate dehydrogenase 1	*Glud1*	11	14
Aconitate hydratase	*Aco2*	6	5
Trifunctional enzyme subunit alpha	*Hadha*	5	7
Malate dehydrogenase	*Mdh2*	5	6
Citrate synthase	*Cs*	4	3
Trifunctional enzyme subunit beta	*Hadhb*	3	5
Isocitrate dehydrogenase [NADP]	*Idh2*	3	10
4-aminobutyrate aminotransferase	*Abat*	2	2
Short/branched chain specific acyl-CoA dehydrogenase	*Acadsb*	2	2
ATP synthase subunit beta	*Atp5b*	2	6
Succinyl-CoA:3-ketoacid coenzyme A transferase 1	*Oxct1*	2	
Protein NipSnap homolog 3B	*Nipsnap3b*	2	3
Succinate dehydrogenase flavoprotein subunit	*Sdha*	2	7
3-ketoacyl-CoA thiolase	*Acaa2*	1	14
Acyl-CoA dehydrogenase family member 10	*Acad10*	1	1
Long-chain specific acyl-CoA dehydrogenase	*Acadl*	1	2
Medium-chain specific acyl-CoA dehydrogenase	*Acadm*	1	2
Acetyl-CoA acetyltransferase	*Acat1*	1	5
Acyl-coenzyme A thioesterase 13	*Acot13*	1	1
Acyl-CoA synthetase family member 2	*Acsf2*	1	1
GTP:AMP phosphotransferase AK3	*Ak3*	1	1
Alpha-aminoadipic semialdehyde dehydrogenase	*Aldh7a1*	1	1
ATP synthase subunit O	*Atp5o*	1	6
Carbonic anhydrase 5B	*Ca5b*	1	
ES1 protein homolog	*D10Jhu81e*	1	1
Dihydrolipoyl dehydrogenase	*Dld*	1	8
Delta(3,5)-Delta(2,4)-dienoyl-CoA isomerase	*Ech1*	1	1
Enoyl-CoA hydratase	*Echs1*	1	2
Enoyl-CoA delta isomerase 2	*Eci2*	1	1
Aspartate aminotransferase	*Got2*	1	12
Isocitrate dehydrogenase [NAD] subunit gamma1	*Idh3a*	1	
Malonyl-CoA-acyl carrier protein transacylase	*Mcat*	1	1
3-mercaptopyruvate sulfurtransferase	*Mpst*	1	1
NAD kinase 2	*Nadk2*	1	
Cysteine desulfurase	*Nfs1*	1	1
Presequence protease	*Pitrm1*	1	
Thiosulfate sulfurtransferase	*Tst*	1	3
Kynurenine/alpha-aminoadipate aminotransferase	*Aadat*		2
Alpha-aminoadipic semialdehyde synthase	*Aass*		2
Short-chain specific acyl-CoA dehydrogenase	*Acads*		3

Cytoplasmic aconitate hydratase	*Aco1*		1
Acyl-coenzyme A synthetase ACSM1	*Acsm1*		3
Acyl-coenzyme A synthetase ACSM3	*Acsm3*		1
Acyl-coenzyme A synthetase ACSM5	*Acsm5*		1
Alcohol dehydrogenase 1	*Adh1*		1
Agmatinase	*Agmat*		2
Serine--pyruvate aminotransferase	*Agxt*		2
Alanine--glyoxylate aminotransferase 2	*Agxt2*		1
Aldehyde dehydrogenase X	*Aldh1b1*		3
Cytosolic 10-formyltetrahydrofolate dehydrogenase	*Aldh1l1*		1
Delta-1-pyrroline-5-carboxylate dehydrogenase	*Aldh4a1*		7
Methylmalonate-semialdehyde dehydrogenase	*Aldh6a1*		3
4-trimethylaminobutyraldehyde dehydrogenase	*Aldh9a1*		2
Alpha-methylacyl-CoA racemase	*Amacr*		1
NAD(P)H-hydrate epimerase	*Apoa1bp*		1
Arginase-1	*Arg1*		1
ATPase family AAA domain-containing protein 3	*Atad3*		1
ATP synthase subunit alpha	*Atp5a1*		5
ATP synthase subunit gamma	*Atp5c1*		1
ATP synthase subunit delta	*Atp5d*		1
ATP synthase subunit epsilon	*Atp5e*		1
ATP synthase F(0) complex subunit B1	*Atp5f1*		4
ATP synthase subunit d	*Atp5h*		7
ATP synthase-coupling factor 6	*Atp5j*		1
ATP synthase subunit f	*Atp5j2*		1
ATP synthase subunit g	*Atp5l*		2
Methylglutaconyl-CoA hydratase	*Auh*		3
D-beta-hydroxybutyrate dehydrogenase	*Bdh1*		1
Valacyclovir hydrolase	*Bphl*		4
Carboxylesterase 1D	*Ces1d*		1
CDGSH iron-sulfur domain-containing protein 3	*Cisd3*		1
Ubiquinone biosynthesis O-methyltransferase	*Coq3*		1
Ubiquinone biosynthesis monooxygenase COQ6	*Coq6*		1
Cytochrome c oxidase subunit 4 isoform 1	*Cox4i1*		1
Cytochrome c oxidase subunit 5B	*Cox5b*		1
Carbamoyl-phosphate synthase	*Cps1*		36
Cytochrome c, somatic	*Cycs*		1
Sterol 26-hydroxylase	*Cyp27a1*		3
Lipoamide acyltransferase	*Dbt*		3
D-dopachrome decarboxylase	*Ddt*		3
2,4-dienoyl-CoA reductase	*Decr1*		3
Probable 2-oxoglutarate dehydrogenase E1 component	*Dhtkd1*		1
Dihydrolipoyllysine-residue acetyltransferase	*Dlat*		1

Dihydrolipoyllysine-residue succinyltransferase	*Dlst*		1
Dimethylglycine dehydrogenase	*Dmgdh*		8
Enoyl-CoA delta isomerase 1	*Eci1*		1
Elongation factor 1-alpha 1	*Eef1a1*		1
Peroxisomal bifunctional enzyme	*Ehhadh*		1
Electron transfer flavoprotein subunit alpha	*Etfa*		4
Electron transfer flavoprotein subunit beta	*Etfb*		2
Electron transfer flavoprotein-ubiquinone oxidoreductase	*Etfdh*		1
Persulfide dioxygenase ETHE1	*Ethe1*		1
Ferrochelatase	*Fech*		2
Fumarate hydratase	*Fh*		4
2-amino-3-ketobutyrate coenzyme A ligase	*Gcat*		3
Glutamine synthetase	*Glul*		1
Glycine N-acyltransferase	*Glyat*		3
Glycine N-acyltransferase-like protein	*Gm4952*		3
Glutathione peroxidase 1	*Gpx1*		4
Glutathione S-transferase A3	*Gsta3*		1
Glutathione S-transferase kappa 1	*Gstk1*		4
Glutathione S-transferase P 1	*Gstp1*		1
Maleylacetoacetate isomerase	*Gstz1*		1
L-gulonolactone oxidase	*Gulo*		1
Hydroxyacyl-coenzyme A dehydrogenase	*Hadh*		3
Hydroxyacylglutathione hydrolase	*Hagh*		1
Haloacid dehalogenase-like hydrolase domain-containing protein 3	*Hdhd3*		1
3-hydroxyisobutyrate dehydrogenase	*Hibadh*		2
3-hydroxyisobutyryl-CoA hydrolase	*Hibch*		1
Histidine triad nucleotide-binding protein 2	*Hint2*		1
Hydroxymethylglutaryl-CoA lyase	*Hmgcl*		1
Hydroxymethylglutaryl-CoA synthase	*Hmgcs2*		9
3-hydroxyacyl-CoA dehydrogenase type-2	*Hsd17b10*		4
3 beta-hydroxysteroid dehydrogenase type 5	*Hsd3b5*		2
Stress-70 protein	*Hspa9*		3
60 kDa heat shock protein	*Hspd1*		6
10 kDa heat shock protein	*Hspe1*		3
Putative transferase CAF17 homolog	*Iba57*		1
Isovaleryl-CoA dehydrogenase	*Ivd*		3
Glycine N-acyltransferase-like protein Keg1	*Keg1*		2
L-2-hydroxyglutarate dehydrogenase	*L2hgdh*		1
Acyl-protein thioesterase 1	*Lypla1*		1
Methylcrotonoyl-CoA carboxylase subunit alpha	*Mccc1*		1
Mitochondrial calcium uniporter regulator 1	*Mcur1*		1
Trans-2-enoyl-CoA reductase	*Mecr*		1
Methylmalonyl-CoA mutase	*Mut*		1

NADH dehydrogenase 1 alpha subcomplex subunit 5	*Ndufa5*		3
NADH dehydrogenase 1 alpha subcomplex subunit 6	*Ndufa6*		1
NADH-ubiquinone oxidoreductase 75 kDa subunit	*Ndufs1*		3
Protein NipSnap homolog 1	*Nipsnap1*		4
Omega-amidase NIT2	*Nit2*		1
Ornithine carbamoyltransferase	*Otc*		5
3-oxoacyl-[acyl-carrier-protein] synthase	*Oxsm*		1
Pyruvate carboxylase	*Pc*		3
Pterin-4-alpha-carbinolamine dehydratase 2	*Pcbd2*		1
Propionyl-CoA carboxylase alpha chain	*Pcca*		1
Peroxisomal trans-2-enoyl-CoA reductase	*Pecr*		1
Prohibitin	*Phb*		1
Inorganic pyrophosphatase 2	*Ppa2*		1
Peroxiredoxin-5	*Prdx5*		1
Proline synthase co-transcribed bacterial homolog protein	*Prosc*		1
60S ribosomal protein L11	*Rpl11*		1
Sarcosine dehydrogenase	*Sardh*		4
Calcium-binding mitochondrial carrier protein Aralar1	*Slc25a12*		2
Calcium-binding mitochondrial carrier protein Aralar2	*Slc25a13*		4
Mitochondrial glutamate carrier 1	*Slc25a22*		1
Phosphate carrier protein	*Slc25a3*		2
ADP/ATP translocase 2	*Slc25a5*		4
Superoxide dismutase [Mn]	*Sod2*		5
Succinyl-CoA ligase [ADP-forming] subunit beta	*Sucla2*		1
Succinyl-CoA ligase [ADP/GDP-forming] subunit alpha	*Suclg1*		3
Succinate-hydroxymethylglutarate CoA-transferase	*Sugct*		1
Mitochondrial import inner membrane translocase subunit Tim13	*Timm13*		1
Cytochrome b-c1 complex subunit 7	*Uqcrb*		4
Cytochrome b-c1 complex subunit 1	*Uqcrc1*		1
Cytochrome b-c1 complex subunit 2	*Uqcrc2*		1
Cytochrome b-c1 complex subunit 6	*Uqcrh*		1
Cytochrome b-c1 complex subunit 8	*Uqcrq*		1
Zinc-binding alcohol dehydrogenase domain-containing protein 2	*Zadh2*		1

[1] PRIDE-dataset identifier PXD007881.
Green: total number of Kglu sites of glutarylated proteins identified in mitochondrial extracts from *Gcdh* KO mouse brain and liver.
Red: non-glutarylated proteins in mitochondrial extracts from *Gcdh* KO mouse brain or liver.

Table S2 -Enrichment analysis of KEGG pathways of *Gcdh* KO brain (A) and liver (B). Related to Figure 4 and Figure S4

A

Term	Pathway	Genes	P-Value	-Log10P
mmu01130	Biosynthesis of antibiotics	GOT2, SDHA, ACAA2, ALDH7A1, ACADM, ACO2, DLD, CS, AK3, IDH2, ECHS1, ACAT1, IDH3A, HADHA, MDH2, HADHB	1.40E-16	15.854
mmu01100	Metabolic pathways	ACADSB, GLUD1, ATP5B, NFS1, ECHS1, ACAT1, HADHA, HADHB, GOT2, IDH2, ATP5O, ACAA2, NADK2, ACADM, ACO2, CS, MCAT, ACADL, IDH3A, SDHA, TST, ALDH7A1, DLD, ABAT, MDH2, MPST	2.80E-16	15.553
mmu00280	Valine, leucine and isoleucine degradation	ACAA2, ALDH7A1, ACADSB, ACADM, OXCT1, DLD, ABAT, ECHS1, ACAT1, HADHA, HADHB	2.50E-15	14.602
mmu01200	Carbon metabolism	GOT2, SDHA, ACADM, ACO2, GLUD1, DLD, CS, IDH2, ECHS1, ACAT1, MDH2, HADHA, IDH3A	3.20E-15	14.495
mmu00071	Fatty acid degradation	ACAA2, ECI2, ALDH7A1, ACADSB, ACADM, ECHS1, ACADL, ACAT1, HADHA, HADHB	7.00E-14	13.155
mmu01212	Fatty acid metabolism	ACAA2, ACADSB, ACADM, MCAT, ECHS1, ACADL, ACAT1, HADHA, HADHB	7.90E-12	11.102
mmu00020	Citrate cycle (TCA cycle)	SDHA, ACO2, DLD, CS, IDH2, MDH2, IDH3A	1.40E-09	8.854
mmu01210	2-Oxocarboxylic acid metabolism	GOT2, ACO2, CS, IDH2, IDH3A	6.00E-07	6.222
mmu00640	Propanoate metabolism	ACADM, ABAT, ECHS1, ACAT1, HADHA	2.70E-06	5.569
mmu00650	Butanoate metabolism	OXCT1, ABAT, ECHS1, ACAT1, HADHA	2.70E-06	5.569
mmu00630	Glyoxylate and dicarboxylate metabolism	ACO2, DLD, CS, ACAT1, MDH2	3.60E-06	5.444
mmu00410	beta-Alanine metabolism	ALDH7A1, ACADM, ABAT, ECHS1, HADHA	6.10E-06	5.215

mmu01230	Biosynthesis of amino acids	GOT2, ALDH7A1, ACO2, CS, IDH2, IDH3A	9.10E-06	5.041
mmu00062	Fatty acid elongation	ACAA2, ECHS1, HADHA, HADHB	1.20E-04	3.921
mmu00620	Pyruvate metabolism	ALDH7A1, DLD, ACAT1, MDH2	4.00E-04	3.398
mmu00270	Cysteine and methionine metabolism	TST, GOT2, MDH2, MPST	4.30E-04	3.367
mmu04122	Sulfur relay system	TST, NFS1, MPST	6.00E-04	3.222
mmu00380	Tryptophan metabolism	ALDH7A1, ECHS1, ACAT1, HADHA	6.90E-04	3.161
mmu00310	Lysine degradation	ALDH7A1, ECHS1, ACAT1, HADHA	9.30E-04	3.032
mmu00250	Alanine, aspartate and glutamate metabolism	GOT2, GLUD1, ABAT	8.40E-03	2.076

B

Term	Pathway	Genes	P-Value	-Log10P
mmu00280	Valine, leucine and isoleucine degradation	HSD17B10, ACADSB, EHHADH, ECHS1, ACAT1, HIBADH, HADHA, AUH, HADHB, MUT, IVD, MCCC1, HADH, HMGCL, ACAA2, ALDH6A1, ACADM, ACADS, DBT, ALDH7A1, HMGCS2, ALDH1B1, DLD, ABAT, HIBCH, ALDH9A1, PCCA	1.30E-33	32.886
mmu01130	Biosynthesis of antibiotics	HSD17B10, EHHADH, ECHS1, AASS, AGXT, ACAT1, HADHA, HADHB, GOT2, ARG1, IDH2, SUCLA2, HADH, AADAT, ACAA2, DLST, ACADM, ACO2, ACO1, SUCLG1, OTC, CS, AK3, DLAT, SDHA, DBT, ALDH7A1, HMGCS2, ALDH1B1, DLD, PCCA, ALDH9A1, MDH2	2.30E-23	22.638
mmu01200	Carbon metabolism	EHHADH, GLUD1, ECHS1, AGXT, ACAT1, HADHA, GOT2, MUT, IDH2, SUCLA2, ALDH6A1, DLST, ACADM, ACO2, ACADS, ACO1, SUCLG1, CS, DLAT, CPS1, SDHA, DLD, HIBCH, MDH2, PCCA	4.80E-21	20.319
mmu00071	Fatty acid degradation	ECI1, ACAA2, ECI2, ACADSB, ACADM, ACADS, EHHADH, ECHS1, ACADL, ACAT1, HADHA, HADHB, ALDH7A1, ALDH1B1, ADH1, HADH, ALDH9A1	8.90E-18	17.051
mmu00650	Butanoate metabolism	ACADS, EHHADH, ECHS1, ACAT1, HADHA, ACSM3, ACSM1, HMGCS2, L2HGDH, ABAT, HADH, BDH1, HMGCL, ACSM5	2.60E-17	16.585

mmu00190	Oxidative phosphorylation	UQCRC2, ATP5D, ATP5E, NDUFA5, ATP5J2, UQCRC1, ATP5B, NDUFA6, ATP5F1, COX4I1, COX5B, UQCRQ, PPA2, SDHA, UQCRH, ATP5C1, ATP5L, ATP5O, ATP5A1, ATP5H, NDUFS1, ATP5J, UQCRB	1.00E-16	16.000
mmu05012	Parkinson's disease	UQCRC2, ATP5D, ATP5E, NDUFA5, UQCRC1, SLC25A5, ATP5B, NDUFA6, CYCS, ATP5F1, COX4I1, COX5B, UQCRQ, SDHA, UQCRH, ATP5C1, ATP5O, ATP5A1, ATP5H, NDUFS1, ATP5J, UQCRB	6.70E-15	14.174
mmu01212	Fatty acid metabolism	ACAA2, ACADSB, ACADM, ACADS, EHHADH, MCAT, ECHS1, ACADL, ACAT1, HADHA, OXSM, HADHB, PECR, HADH, MECR	1.80E-14	13.745
mmu00640	Propanoate metabolism	ALDH6A1, MUT, ACADM, SUCLG1, EHHADH, ABAT, ECHS1, HIBCH, SUCLA2, ACAT1, HADHA, PCCA	8.50E-14	13.071
mmu05016	Huntington's disease	UQCRC2, ATP5D, ATP5E, NDUFA5, UQCRC1, SLC25A5, ATP5B, NDUFA6, CYCS, ATP5F1, COX4I1, COX5B, UQCRQ, SOD2, SDHA, UQCRH, ATP5C1, ATP5O, ATP5A1, ATP5H, NDUFS1, ATP5J, UQCRB	2.20E-13	12.658
mmu05010	Alzheimer's disease	UQCRC2, ATP5D, HSD17B10, ATP5E, NDUFA5, UQCRC1, ATP5B, NDUFA6, CYCS, ATP5F1, COX4I1, COX5B, UQCRQ, SDHA, UQCRH, ATP5C1, ATP5O, ATP5A1, ATP5H, NDUFS1, ATP5J, UQCRB	2.20E-13	12.658
mmu00020	Citrate cycle (TCA cycle)	SDHA, DLST, ACO2, ACO1, SUCLG1, DLD, CS, IDH2, DLAT, SUCLA2, MDH2	2.70E-11	10.569
mmu00630	Glyoxylate and dicarboxylate metabolism	MUT, GLUL, ACO2, ACO1, DLD, CS, ACAT1, AGXT, MDH2, PCCA	3.00E-10	9.523
mmu00410	beta-Alanine metabolism	ALDH6A1, ALDH7A1, ACADM, ALDH1B1, EHHADH, ABAT, ECHS1, HIBCH, ALDH9A1, HADHA	1.10E-09	8.959
mmu00310	Lysine degradation	AADAT, DLST, ALDH7A1, ALDH1B1, EHHADH, ECHS1, AASS, HADH, ACAT1, ALDH9A1, HADHA	5.20E-09	8.284
mmu00250	Alanine, aspartate and glutamate metabolism	GOT2, GLUL, NIT2, GLUD1, ABAT, ALDH4A1, AGXT2, CPS1, AGXT	7.10E-08	7.149
mmu01230	Biosynthesis of amino acids	AADAT, GOT2, ARG1, ALDH7A1, GLUL, ACO2, ACO1, OTC, CS, IDH2, CPS1	2.90E-07	6.538
mmu00380	Tryptophan metabolism	AADAT, ALDH7A1, ALDH1B1, EHHADH, ECHS1, HADH, ACAT1, ALDH9A1, HADHA	5.10E-07	6.292
mmu04146	Peroxisome	PECR, ECI2, ECH1, GSTK1, EHHADH, AMACR, IDH2, PRDX5, AGXT,	5.30E-07	6.276

		HMGCL, SOD2		
mmu00620	Pyruvate metabolism	HAGH, ALDH7A1, ALDH1B1, DLD, DLAT, ACAT1, ALDH9A1, MDH2	1.90E-06	5.721
mmu00220	Arginine biosynthesis	GOT2, ARG1, GLUL, OTC, GLUD1, CPS1	8.20E-06	5.086
mmu01210	2-Oxocarboxylic acid metabolism	AADAT, GOT2, ACO2, ACO1, CS, IDH2	8.20E-06	5.086
mmu04932	Non-alcoholic fatty liver disease (NAFLD)	UQCRC2, SDHA, NDUFA5, UQCRC1, UQCRH, NDUFA6, CYCS, COX4I1, COX5B, UQCRQ, NDUFS1, UQCRB	3.00E-05	4.523
mmu00260	Glycine, serine and threonine metabolism	ALDH7A1, DLD, GCAT, DMGDH, AGXT2, SARDH, AGXT	3.10E-05	4.509
mmu00062	Fatty acid elongation	ACAA2, ECHS1, HADH, MECR, HADHA, HADHB	4.20E-05	4.377
mmu00330	Arginine and proline metabolism	GOT2, ARG1, ALDH7A1, ALDH1B1, ALDH4A1, AGMAT, ALDH9A1	1.00E-04	4.000
mmu00920	Sulfur metabolism	TST, ETHE1, CYCS, MPST	5.50E-04	3.260
mmu00072	Synthesis and degradation of ketone bodies	HMGCS2, ACAT1, BDH1, HMGCL	5.50E-04	3.260
mmu04260	Cardiac muscle contraction	UQCRC2, UQCRC1, UQCRH, COX4I1, COX5B, UQCRQ, UQCRB	1.20E-03	2.921
mmu00010	Glycolysis / Gluconeogenesis	ALDH7A1, ADH1, ALDH1B1, DLD, DLAT, ALDH9A1	3.50E-03	2.456
mmu00360	Phenylalanine metabolism	GOT2, GLYAT, GM4952, KEG1	5.20E-03	2.284
mmu00053	Ascorbate and aldarate metabolism	ALDH7A1, ALDH1B1, GULO, ALDH9A1	8.20E-03	2.086
mmu04122	Sulfur relay system	TST, NFS1, MPST	9.90E-03	2.004

KEGG pathway enrichment analysis (Kanehisa & Goto, 2000) was performed using DAVID (The Database for Annotation, Visualization and Integrated Discovery) tools with the total mouse genome information as the background (Huang et al, 2009). The adjusted p-value cutoff is <0.01.

Table S3 – Time- (A) and glu-CoA-dependent (B) progression of lysine glutarylation of *in vitro* glutarylated bovine GDH. Related to Figure S6 and Figure S9.

A

glu-CoA concentration (mM)		0	5.0	5.0	5.0
Time (h)		0	1	2	4
Kglu sequence (including sub-sequences)	Kglu position	Sum of Area [a]	Sum of Area [a]	Sum of Area [a]	Sum of Area [a]
[R].GASIVEDKLVEDLK.[T]	84	1.7E+06	9.6E+07	2.0E+08	6.7E+08
[R].GASIVEDKLVEDLKTR.[E]	84/90		2.8E+07	1.3E+08	4.2E+08
[K].GGIRYSTDVSVDEVKALASLMTYK.[C]	162	9.6E+06	4.7E+08	1.1E+09	3.2E+09
[K].ALASLMTYKCAVVDVPFGGAK.[A]	171		3.4E+07	1.1E+08	2.2E+08
[K].CAVVDVPFGGAKAGVKINPK.[N]	183		9.6E+07	6.7E+08	9.1E+08
[K].INPKNYTDNELEK.[I]	191		2.0E+08	2.2E+09	4.5E+09
[K].NYTDNELEKITR.[R]	200		5.3E+07	3.0E+08	8.0E+08
[K].INPKNYTDNELEKITR.[R]	191+200			9.8E+06	2.7E+07
[K].KGFIGPGVDVPAPDMSTGER.[E]	212			2.1E+07	5.2E+07
[K].ELEDFKLQHGTILGFPK.[A]	352		8.8E+07	2.1E+08	1.7E+09
[K].AKIYEGSILEVDCDILIPAASEK.[Q]	365		5.7E+07	1.4E+08	2.2E+08
[K].ELEDFKLQHGTILGFPKAK.[I]	352+363/365			4.3E+06	1.2E+08
[K].IYEGSILEVDCDILIPAASEKQLTK.[S]	386		2.2E+07	4.3E+07	3.5E+07
[K].AKIIAEGANGPTTPEADKIFLER.[N]	399	6.6E+06	3.1E+07	7.1E+07	9.0E+08
[R].VKAKIIAEGANGPTTPEADK.[I]	397/399				2.0E+06
[K].IIAEGANGPTTPEADKIFLER.[N]	415	1.7E+07	1.3E+08	5.5E+08	1.5E+09
[K].FGKHGGTIPIVPTAEFQDR.[I]	480		1.1E+08	4.8E+08	3.8E+09
[R].KFGKHGGTIPIVPTAEFQDR.[I]	477/480		2.2E+07	2.9E+08	3.0E+09
[R].ISGASEKDIVHSGLAYTMER.[S]	503	8.2E+06	1.8E+08	3.1E+09	7.6E+09
[R].TAMKYNLGLDLR.[T]	527		1.1E+08	9.6E+08	2.0E+09
[R].TAAYVNAIEKVFR.[V]	545	1.5E+07	3.1E+07	8.0E+07	2.0E+08
Total GDH Kglu peptide intensity	**all**	**5.8E+07**	**1.8E+09**	**1.1E+10**	**3.2E+10**

B

glu-CoA concentration (mM)		0	0.5	1.0	5.0
Time (h)		0	4	4	4
Kglu sequence (including sub-sequences)	Kglu position	Sum of Area [a]	Sum of Area [a]	Sum of Area [a]	Sum of Area [a]
[R].GASIVEDKLVEDLK.[T]	84	1.7E+06	9.4E+07	1.8E+08	6.7E+08
[R].GASIVEDKLVEDLKTR.[E]	84/90		3.5E+07	1.0E+08	4.2E+08
[K].GGIRYSTDVSVDEVKALASLMTYK.[C]	162	9.6E+06	3.5E+08	6.9E+08	3.2E+09
[K].ALASLMTYKCAVVDVPFGGAK.[A]	171		2.1E+07	6.4E+07	2.2E+08
[K].CAVVDVPFGGAKAGVKINPK.[N]	183		1.1E+08	1.6E+08	9.1E+08
[K].INPKNYTDNELEK.[I]	191		7.3E+08	3.7E+08	4.5E+09
[K].NYTDNELEKITR.[R]	200		1.1E+08	1.0E+08	8.0E+08
[K].INPKNYTDNELEKITR.[R]	191+200				2.7E+07
[K].KGFIGPGVDVPAPDMSTGER.[E]	212				5.2E+07
[K].ELEDFKLQHGTILGFPK.[A]	352		4.2E+07	1.5E+08	1.7E+09
[K].AKIYEGSILEVDCDILIPAASEK.[Q]	365		3.3E+07	9.6E+07	2.2E+08
[K].ELEDFKLQHGTILGFPKAK.[I]	352+363/365				1.2E+08
[K].IYEGSILEVDCDILIPAASEKQLTK.[S]	386		1.4E+07	4.5E+07	3.5E+07

[K].AKIIAEGANGPTTPEADKIFLER.[N]	399	6.6E+06	4.8E+07	3.9E+07	9.0E+08
[R].VKAKIIAEGANGPTTPEADK.[I]	397/399				2.0E+06
[K].IIAEGANGPTTPEADKIFLER.[N]	415	1.7E+07	1.5E+08	2.8E+08	1.5E+09
[K].FGKHGGTIPIVPTAEFQDR.[I]	480		1.8E+08	9.9E+07	3.8E+09
[R].KFGKHGGTIPIVPTAEFQDR.[I]	477/480		2.0E+07	2.9E+07	3.0E+09
[R].ISGASEKDIVHSGLAYTMER.[S]	503	8.2E+06	1.3E+09	1.2E+09	7.6E+09
[R].TAMKYNLGLDLR.[T]	527		3.5E+08	2.8E+08	2.0E+09
[R].TAAYVNAIEKVFR.[V]	545	1.5E+07	4.8E+07	7.3E+07	2.0E+08
Total GDH Kglu peptide intensity	**all**	**5.8E+07**	**3.6E+09**	**4.0E+09**	**3.2E+10**

[a] Peak areas of extracted ion chromatograms of all found Kglu-peptides were listed.

Supplemental Experimental Procedures

Antibodies. Rabbit anti-human GCDH antibody was kindly provided by Dr. S. I. Goodman (University of Colorado Health Sciences Center, Denver). Pan polyclonal anti-glutaryllysine antibody (#PTM-1151, Kglu) used for electron and immunofluorescence microscopy, was purchased from PTM Biolabs. The polyclonal goat anti-GDH antibody (#ab99470), rabbit anti-ETFB (#ab73986), the monoclonal rabbit anti-Sirt5 (#ab108968) and mouse anti-Atp5b (#ab14730) were purchased from Abcam (Cambridge, UK). The monoclonal mouse anti-α-tubulin (#T9026) and polyclonal mouse anti-DLST (#SAB1400079 antibody) were obtained from Sigma-Aldrich (Munich, Germany), rabbit anti-MnSOD (#06-984) and mouse anti-NeuN antibodies (#MAB377) from Millipore (Billerica, USA), and polyclonal rabbit anti-GFAP (#N1506) from DAKO (Hamburg, Germany).
The monoclonal mouse anti-α-GM130 antibody was purchased from BD Biosciences (San Jose, CA, USA) and the monoclonal mouse anti-PDI antibody from Enzo Life Sciences (Farmingdale, NY, USA). The polyclonal rabbit antibodies against mouse Ca5b, human CAII and human CAIV were described recently (Hu et al, 1995; Shah et al, 2000; Waheed et al, 1997). HRP-conjugated anti-V5 antibody, monkey anti-mouse IgG coupled to Alexa Fluor 488 and goat anti-rabbit IgG coupled to Alexa Fluor 546 were from Invitrogen (Karlsruhe, Germany). Donkey anti-rabbit IgG coupled to AlexaFluor 488 and Cy3-donkey anti-mouse IgG were obtained from Jackson ImmunoResearch Dianova (Hamburg, Germany). Protein A gold secondary antibody was purchased from G. Posthuma (University Medical Center Utrecht).

Generation of glutaryl-lysine-specific antibodies.
Polyclonal glutaryl-lysine specific antibodies were generated by immunizing a New Zealand White rabbit (K14117) using *in vitro* glutarylated ovalbumin. The animal received five s.c. immunizations in three week intervals with 200 µg antigen emulsified in Stimune adjuvant (Thermo Fisher) per injection. Serum was prepared 14 days after the final boost and specificity was verified by ELISA using *in vitro* glutarylated albumin (titer 1:30.000) and unmodified albumin (titre < 1:50). IgG was purified from serum by affinity chromatography on a protein G sepharose column (GE-Healthcare). Bound IgG was eluted from the column with 100 mM Tris-glycine, pH 2.7. The eluate was immediately neutralized by addition of 1/10th volume 1 M Tris pH 9.0 and the buffer was exchanged for PBS by gel filtration using a PD-10 column (GE Healthcare). Purified antibody was used in all western blot analyses.

Reagents. The following reagents were obtained commercially as indicated:
Glutamate Dehydrogenase Activity Assay Kit; purified L-glutamate dehydrogenase from bovine liver, citraconic anhydride, protease inhibitor mixture, DNase I, papain, ovalbumin and AraC were purchased from Sigma-Aldrich (Munich, Germany); human recombinant SIRT5 (His-tag) expressed in *E. coli* and Amicon Ultra-Centrifugal Filter with Ultracel-10 membrane from Merck-Millipore (Billerica, USA); DMEM, 2-D Quant Kit, Immobiline DryStrip gels pH 3-10 and Protein G Sepharose 4 Fast Flow from GE Healthcare (Freiburg, Germany); enhanced chemiluminescence reagents (ECL) and DRAQ5™ Fluorescent Probe Solution from Thermo Scientific (Waltham, USA); Minimal essential medium (MEM), Dulbecco's minimal essential medium (DMEM), fetal calf serum (FCS), trypsin/EDTA, B27 supplement, penicillin/streptomycin, neurobasal A medium and horse serum from Invitrogen (Karlsruhe, Germany); IEF gel electrophoresis Criterion™ IEF Precast Gels (pH 3-10), IEF sample buffer, 10x IEF Cathode Buffer and 10x IEF Anode Buffer from BioRad (Munich, Germany); IEF marker (pH 3-10) from SERVA (Heidelberg, Germany); Roti®quant Protein Assay from Roth (Karlsruhe, Germany); Aqua-Poly/Fluoromount from Polysciences (Warrington, USA); Carbon-Formvar-coated nickel grids from Science Services GmbH (Munich, Germany).

Animal experiments. GCDH-deficient mice and wild-type littermate controls were generated from heterozygotes (Koeller et al, 2002). The genetic background of all mice groups used in this study was C57BL6/SJ129 hybrid. The genotypes were confirmed by polymerase chain reaction (PCR). The mice were housed in an animal facility of the University Hospital with a 12-h light–dark cycle and allowed water and food ad libitum. Animal care was provided in accordance with institutional guidelines. Thirty-eight days old wild-type (WT) and *Gcdh*-deficient (KO) mice were maintained on a normal chow diet (ND) or a high protein diet (HPD) containing 70% casein purchased from Harlan Laboratories (Indianapolis, IN, USA) for four days. Except for the age-dependent western blot analysis, all animals used were sacrificed at the age of 6 weeks.

Electron microscopy:
Animals were deeply anaesthetized by a mixture of ketanest and rompun and perfused through the heart with 4% paraformaldehyde (w/v) and 0.1 % glutaraldehyde (w/v) in 0.1M phosphate buffer, pH 7.2. One hundred µm thick vibratome sections of the cerebellum were prepared. For post-embedding immunogold labeling, small pieces of cryoprotected cerebellar tissue (2.3 M sucrose) were mounted on specimen holders immersed in liquid nitrogen and ultrathin sections (70 nm) were cut and labeled as described previously (Slot & Geuze, 2007). Briefly, sections were collected on Carbon-Formvar-coated nickel grids. Rabbit anti-Kglu dilution 1:250 was

recognized with 10 and 15 nm large protein A gold secondary antibodies. Ultrathin sections were examined using an EM902 (Zeiss, Germany). Pictures were taken with a TRS 2K digital camera (A. Tröndle, Moorenweis, Germany).

Immunofluorescence and confocal microscopy. For double immunofluorescence microscopy, primary cells were grown on glass coverslips. Cells were fixed with 4 % paraformaldehyde in PBS for 30 min, washed with PBS, permeabilized with 1 % Triton X-100 in PBS for 10 min and blocked with PBS containing 3 % BSA. After blocking, cells were subsequently incubated with primary antibodies and secondary antibodies conjugated to Alexa Fluor® 546 and Alexa Fluor® 488 for 1 h each. After embedding in Fluoromount-Medium cells were imaged using a 63×/1.32–0.6 oil immersion objective lens on a SP5 confocal microscope (Leica, 63×). The pictures were taken using the Leica LCS software.

Histology and immunohistochemistry in brain and liver of WT and *Gcdh* KO mice. For immunofluorescence, 2 µm paraffin sections were deparaffinized and rehydrated to water. Antigen retrieval was obtained by boiling in 0.05 % citraconic anhydride pH 7.4 for 30 min at constant 98°C. Unspecific binding was blocked with 5 % horse serum containing 0.05 % Triton X-100 (blocking solution) for 30 min at room temperature prior to incubation at 4°C overnight with primary antibodies in blocking solution. Staining was visualized with fluorochrome conjugated secondary antibodies. Nuclei were visualized using Draq5. Negative controls were performed by omitting primary antibodies. Staining's were evaluated with a confocal LSM 510 meta microscope using the LSM software (Zeiss).

Western blot analysis. Solubilized protein extracts were separated on SDS–PAGE, transferred to Protran® nitrocellulose membranes (Whatman, Dassel, Germany), probed with anti-glutaryl-lysine antibody or protein-specific antibodies and visualized with secondary HRP-conjugated goat anti-mouse or goat-anti rabbit IgG antibodies. The immunoreactive bands were visualized by enhanced chemiluminescence.

Two-dimensional gel electrophoresis. Crude mitochondrial fractions isolated from WT and *Gcdh* KO mice were precipitated and quantified using 2-D Quant Kit. Aliquots (25 µg protein) were resuspended in rehydration loading mix (7 M urea, 2 M thiourea, 3 % 3-[(3-cholamidylpropyl)-dimethylammonio]-1-propanesulfonate (CHAPS), 0.002 % bromophenol blue, 184 mM HED, 0.5 % IPG buffer pH 4-7 or pH 6-11 (GE Healthcare)). Samples were adjusted to the final volume of 150 µl and applied to Immobiline DryStrip gels pH 3-10 by passive reswelling overnight. The first dimension was carried out by using a six-step program of 8300 V/h in total. After IEF, IPG strips were reduced and alkylated by incubation in equilibration buffer (6 M urea, 50 mM Tris-HCl [pH 8.8], 30 % glycerol, 2 % [wt/vol] sodium dodecyl sulfate [SDS]) containing dithiothreitol (10 mg/ml) or iodoacetamide (25 mg/ml) for 22 min at room temperature. The second dimension polyacrylamide gel electrophoresis (PAGE) was carried out with 5 mA overnight on self-cast SDS-polyacrylamide gels using the following running parameters: 2.5 mA for 45 min, 5 mA for 45 min, 10 mA for 30 min and 20 mA until the migration front reached the edge of the gel followed by electroblotting onto nitrocellulose membrane, blocking and ECL-mediated immunodetection.

Preparation of hepatocytes. Primary mouse hepatocytes were isolated by liver perfusion, EDTA dissociation and centrifugation on a Percoll gradient according to Meredith (Meredith, 1988).

Isolation of mitochondria from different mouse organs. Tissues were collected and homogenized immediately on ice by using a glass potter. Liver and brain tissue were homogenized with 4 strokes and a rotating Teflon pestle operated at 1,600 r.p.m. Eight strokes were used for homogenization of kidney and spleen tissue. The homogenization buffer contained 10 mM Tris–MOPS, pH 7.4 buffer containing 1 mM EGTA/Tris, 200 mM sucrose and protease inhibitor cocktail. Mitochondria were extracted as described previously (Frezza et al, 2007) and used for western blotting.

Subcellular fractionation. Fractions enriched in cytosolic and mitochondrial marker enzymes were obtained by differential centrifugation as described previously (Cox & Emili, 2006). In brief, mice were sacrificed, livers were removed, homogenized in 5 volumes of ice-cold isotonic sucrose solution (250 mM sucrose), and used for differential centrifugation.
Part of the mitochondrial and cytosolic fractions were glutarylated *in vitro* with 5 mM glutaryl-CoA for 4 h on a rotating wheel at room temperature. Western blot was performed to examine the levels of global lysine glutarylation in the different fractions using anti Kglu antibodies.

Functional annotation of Kglu proteins. Kyoto Encyclopedia of Genes and Genomes (KEGG) pathway (Kanehisa and Goto, 2000) analysis were performed using DAVID (The Database for Annotation, Visualization and Integrated Discovery) tools with the total mouse genome information as the background (Huang da et al, 2009). The adjusted p-value (Benjamini) cutoff is <0.01.

GCDH affinity chromatography. For GCDH affinity chromatography a GCDH affinity matrix was prepared as described previously (Schmiesing et al, 2014). Afterwards purified bovine GDH and recombinant human ETFB or DLST (*in vitro* glutarylated or unglutarylated) were applied to the GCDH-affinity matrix and incubated for 2 h at 4°C on a rotating wheel. Unbound material was discarded, and the column was washed with five volumes ice-cold buffer A (50 mM Hepes, pH 8.0 containing 5 mM KCl and 120 mM NaCl). Ten percent of the input (In) and the total bound (B) material were solubilized and separated on SDS–PAGE for western blot analysis.

GDH activity assay. Enzyme activity measurements were performed with purified glutarylated/non-glutarylated proteins and liver and brain homogenates using a coupled enzyme assay from Sigma-Aldrich (#MAK099). Briefly, 100 mg of liver and brain tissue were homogenized in 200 µl of ice-cold GDH assay buffer containing protease inhibitors with ten strokes in a Potter-Elvejhem homogenizer. After 10 min incubation on ice the samples were centrifuged at 13,000 g for 10 min at 4 °C to remove insoluble material. Supernatants (40 µg protein) of liver/brain samples or 50 ng of purified protein in a final volume of 50 µl GDH assay buffer were added to a 100 µl master reaction mixture and incubated at 37 °C. Every 3 min samples were measured (A450 nm) using the Multiskan GO monochromator-based UV/VIS spectrophotometer from Thermo Fisher Scientific. The reaction was referenced against an NADH standard curve.

Construction of bacterial expression vector containing mouse Ca5b cDNA. A *BamHI-NcoI* DNA fragment from mouse CA5b cDNA was cloned into pET-11a vector and used for pRARE *E. coli* host cell transformation.

Expression and purification of recombinant mouse Ca5b. *E. coli* pRARE (DE3) containing mouse Ca5b were grown at 37°C in LB medium containing 100 µg/ml ampicillin and chloramphenicol to OD 600nm around 0.5. Protein expression was induced by the addition of 0.2 mM IPTG and 0.6 mM $ZnSO_4$, and cultures were grown overnight at 20°C. The cells were recovered after centrifugation at 7000xg for 15 min at 4°C and lysed in lysis buffer as described (Waheed et al, 1997). The clear supernatant was collected after centrifugation of cell lysates at 15000 x g for 30 min at 4°C and applied to a carbonic anhydrase inhibitor affinity column. The bound enzyme was eluted as described (Zhu & Sly, 1990).

***In silico* modeling of 3D Gdh structure.**
A homology model of murine Gdh was generated using Swiss-Model and the structure of bovine GDH (pdb:3etd) as template. Sequence identity is >95%. Surface representation and glutarylated lysine residues were illustrated using PyMOL.

Appendix Supplementary Methods References

Cox B, Emili A (2006) Tissue subcellular fractionation and protein extraction for use in mass-spectrometry-based proteomics. *Nat Protoc* **1:** 1872-1878

Frezza C, Cipolat S, Scorrano L (2007) Organelle isolation: functional mitochondria from mouse liver, muscle and cultured fibroblasts. *Nat Protoc* **2:** 287-295

Huang da W, Sherman BT, Lempicki RA (2009) Bioinformatics enrichment tools: paths toward the comprehensive functional analysis of large gene lists. *Nucleic Acids Res* **37:** 1-13

Kanehisa M, Goto S (2000) KEGG: kyoto encyclopedia of genes and genomes. *Nucleic Acids Res* **28**: 27-30

Koeller DM1, Woontner M, Crnic LS, Kleinschmidt-DeMasters B, Stephens J, Hunt EL, Goodman SI (2002) Biochemical, pathologic and behavioral analysis of a mouse model of glutaric acidemia type I. *Hum Mol Genet* **11**: 347-357

Meredith MJ (1988) Rat hepatocytes prepared without collagenase: prolonged retention of differentiated characteristics in culture. *Cell Biol Toxicol* **4:** 405-425

Schmiesing J, Schlüter H, Ullrich K, Braulke T, Mühlhausen C (2014) Interaction of glutaric aciduria type 1-related glutaryl-CoA dehydrogenase with mitochondrial matrix proteins. *PLoS One* **9:** e87715

Waheed A, Pham T, Won M, Okuyama T, Sly WS (1997) Human carbonic anhydrase IV: in vitro activation and purification of disulfide-bonded enzyme following expression in Escherichia coli. *Protein Expr Purif* **9:** 279-287

Zhu XL, Sly WS (1990) Carbonic anhydrase IV from human lung. Purification, characterization, and comparison with membrane carbonic anhydrase from human kidney. *J Biol Chem* **265:** 8795-8801

Zinnanti WJ, Lazovic J, Wolpert EB, Antonetti DA, Smith MB, Connor JR, Woontner M, Goodman SI, Cheng KC (2006) A diet-induced mouse model for glutaric aciduria type I. *Brain* **129:** 899-910